NASA Technical Memorandum 104412
AIAA-91-2458

Mixing of Multiple Jets With a Confined Subsonic Crossflow

Summary of NASA-Supported Experiments and Modeling

James D. Holdeman
Lewis Research Center
Cleveland, Ohio

Prepared for the
27th Joint Propulsion Conference
cosponsored by AIAA, SAE, ASME, and ASEE
Sacramento, California, June 24-27, 1991

NASA

MIXING OF MULTIPLE JETS WITH A CONFINED SUBSONIC CROSSFLOW
Summary of NASA-Supported Experiments and Modeling

James D. Holdeman*
National Aeronautics and Space Administration
Lewis Research Center
Cleveland, Ohio 44135

Abstract

This paper summarizes experimental and computational results on the mixing of single, double, and opposed rows of jets with an isothermal or variable temperature mainstream in a confined subsonic crossflow. The studies from which these results came were performed to investigate flow and geometric variations typical of the complex three-dimensional flowfield in the dilution zone of combustion chambers in gas turbine engines.

The principal observations from the experiments were that the momentum-flux ratio was the most significant flow variable, and that temperature distributions were similar, independent of orifice diameter, when the orifice spacing and the square-root of the momentum-flux ratio were inversely proportional. The experiments and empirical model for the mixing of a single row of jets from round holes were extended to include several variations typical of gas turbine combustors, namely variable temperature mainstream, flow area convergence, noncircular orifices, and double and opposed rows of jets, both in-line and staggered. All except the last of these were appropriately modeled with superposition or patches to the basic empirical model. Combinations of flow and geometry that gave optimum mixing were identified from the experimental results.

Based on the results of calculations made with a three-dimensional numerical model, the empirical model was further extended to model the effects of curvature and convergence. The principal conclusions from this study were that the orifice spacing and momentum-flux relationships were the same as observed previously in a straight duct, but the jet structure was significantly different for jets injected from the inner wall of a turn than for those injected from the outer wall. Also, curvature in the axial direction caused a drift of the jet trajectories toward the inner wall, but the mixing in a turning and converging channel did not seem to be inhibited by the convergence, independent of whether the convergence was radial or circumferential. The calculated jet penetration and mixing in an annulus were similar to those in a rectangular duct when the orifice spacing was specified at the radius dividing the annulus into equal areas.

*Senior Research Engineer, Aerothermochemistry Branch. Member AIAA.

Nomenclature

A_j/A_m	jet-to-mainstream area ratio; $(\pi/4)/((S/H_0)(H_0/D)^2)$ for one-side injection; $(\pi/2)/((S/H_0)(H_0/D)^2)$ for two-side injection
C	$(S/H_0)\sqrt{(J)}$; Eq. (3)
C_d	orifice discharge coefficient
D	orifice diameter
D_j	$(D)\sqrt{(Cd)}$
DR	jet-to-mainstream density ratio (T_m/T_j)
dH/dx	duct convergence rate
H_{eq}	effective duct height; H_0 except for opposed rows of jets with centerlines in-line; see Appendix
H_0	duct height at injection plane
J	jet-to-mainstream momentum-flux ratio $(DR)(R)^2$
M	jet-to-mainstream mass-flux ratio (DR)(R)
n	number of holes around can; see Eq. (6)
r	radial coordinate
R	jet-to-mainstream velocity ratio (V_j/U_m)
R_{ci}	inner radius of curvature in x-r plane
R_i	inner radius of curvature at inlet in r-z plane
S	spacing between orifice centers
S_x	spacing between orifice rows
T	temperature
T_j	jet exit temperature
T_m	mainstream temperature

U	velocity
U_m	mainstream velocity
V_j	jet velocity
w_j/w_m	$\sqrt{(DR)(J)}\,(C_d)(A_j/A_m)$
w_j/w_T	jet-to-total mass flow ratio; equilibrium θ
	$\dfrac{w_j/w_m}{1 + w_j/w_m}$
$W^{\pm}_{1/2}$	jet half-widths on injection (-) or opposite (+) side of jet centerline; see Fig. 5
x	downstream coordinate; 0 at injection plane
y	cross-stream (radial) coordinate; 0 at wall; y_c at location of minimum temperature in a line x = constant, z = constant
z	lateral (circumferential) coordinate; 0 at centerplane
θ	$(T_m - T)/(T_m - T_j)$; Eq. (1)
θ_c	temperature difference ratio at y_c
$\theta^{\pm}_{min}$	minimum temperature difference ratio on injection (-) or opposite (+) side of jet centerline; see Fig. 5

Introduction

The problem of jets-in-crossflow has been extensively treated in the literature, to the point that it can almost be considered a classical three-dimensional flow problem. Although studies to date have all contributed additional understanding of the general problem, the information obtained in them was determined by their motivating application, and may not satisfy the specific needs of different applications.

Considerations of mixing in gas turbine combustion chambers have, during the past two decades, motivated several studies on the mixing characteristics of jets injected normally into a confined crossflow. These are reported in, e.g., Walker & Kors (1973); Walker, Kors, & Holdeman (1973); Holdeman, Walker, & Kors (1973); Kamotani & Greber (1973, 1974); Walker & Eberhardt (1975); Holdeman, Walker, & Eberhardt (1975); Cox (1975, 1976); Holdeman & Walker (1977); Bruce, Mongia, & Reynolds (1979); Novick, Arvin, & Quinn (1980); Novick & Troth (1981); Lipshitz & Greber (1981), Riddlebaugh, Lipshitz, & Greber (1982); Khan, McGuirk, & Whitelaw (1982); Atkinson, Khan, & Whitelaw (1982); Srinivasan, Berenfeld, & Mongia (1982); Holdeman (1983); Lipshitz & Greber (1984); Holdeman, Srinivasan, & Berenfeld (1984); Wittig, Elbahar, & Noll (1984); Srinivasan, Coleman, & Johnson (1984); Holdeman & Srinivasan (1984); Ferrell, Abujalla, Busnania, & Lilley (1984); Ferrell, Aoki, & Lilley (1985); Ferrell & Lilley (1985a,b); Srinivasan, Meyers, Coleman, & White (1985); Srinivasan & White (1986); Holdeman & Srinivasan (1986a,b); McMurray & Lilley (1986); Ong & Lilley (1986); Lilley (1986); Ong, McMurray, & Lilley (1986); McMurray, Ong, & Lilley (1987); Reynolds & White (1987); Holdeman, Reynolds, & White (1987); Srinivasan & White (1988); Holdeman, Srinivasan, & White (1988); Vranos & Liscinsky (1988); Sullivan, Barron, Seal, Morgan, & Murthy (1989); Nikjooy, Karki, & Mongia (1990); Dwenger (1990); Carrotte & Stevens (1990); Stevens & Carrotte (1990a,b); Richards & Samuelsen (1990a,b,c); Smith (1990); Talpallikar & Smith (1991); Holdeman, Reynolds, Srinivasan, & White (1991), Talpallikar, Smith, Lai, & Holdeman (1991), Vranos & Liscinsky (1991); Vranos, Liscinsky, True, & Holdeman (1991) and Smith, Talpallikar, & Holdeman (1991).

One factor making the combustor dilution zone jet-in-crossflow application unique is that it is a confined mixing problem, with from 10 to 50 percent of the total flow entering through the dilution jets. The result is that the equilibrium temperature of the exiting flow may differ significantly from that of the entering mainstream flow. To control or tailor the combustor exit temperature pattern it is necessary to be able to characterize the exit distribution in terms of the upstream flow and geometric variables. This requires that the entire flowfield be either known or modeled.

Description of the Flowfield

Figure 1 shows a schematic of the flow in a rectangular duct with injection from a row of jets on the top wall. The temperature field results are often presented as plots of the temperature difference ratio, θ, where

$$\theta = \frac{(T_m - T)}{(T_m - T_j)} \qquad (1)$$

A sequence of three-dimensional oblique views of this parameter at several locations downstream of the injection plane is shown in Fig. 2. In these plots the temperature distribution is shown (on the abscissa) in y-z planes normal to the main flow direction, x. The coordinates y and z are, respectively, parallel to the orifice centerlines and the row of orifices. Note that the jet fluid is identified by larger values of θ (i.e., $\theta = 1$ if $T = T_j$, and $\theta = 0$ if $T = T_m$). The equilibrium θ for any configuration is equal to the fraction of the total flow entering through the dilution jets, w_j/w_T. Because the objective in this application was to identify dilution zone configurations to provide a desired mixing pattern within a given combustor length, the downstream stations of interest

were defined in intervals of the duct height at the injection location, H_0, rather than the orifice diameter, D.

The orifice configurations discussed herein are shown in Fig. 3. The primary independent geometric variables for each of these are the spacing between adjacent orifices, S, the orifice diameter, D (for noncircular orifices, this is taken as the diameter of a circle of equal area), and, for double rows, the axial spacing between rows, S_x. These are expressed in dimensionless form as the ratio of the orifice spacing to duct height, S/H_0, the ratio of the duct height to orifice diameter, H_0/D, and the ratio of the axial spacing to the duct height, S_x/H_0.

The basic geometry for the turning and converging ducts in the numerical and empirical studies reported by Holdeman, Srinivasan, Reynolds, & White (1991) is shown in Fig. 4(a). The duct convergence was identified by the ratio of the exit cross-sectional area to that at the jet injection location. The curved sections in the x-r plane were generated using circular arcs, and the curvature parameter was specified as the inner radius of curvature of the duct normalized by the inlet duct height, R_{ci}/H_0. The radius of curvature of the inner duct wall in the r-z plane is given nondimensionally by its ratio to the inlet duct height, R_t/H_0.

Curved and converging ducts are defined by values of R_{ci} and R_t between zero and infinity (see Fig. 4(a)). Some limiting cases of interest are as follows: a rectangular channel is defined if R_t and R_{ci} are infinite; a can results if R_{ci} is infinite and $R_t = 0$; and an annular duct results if R_{ci} is infinite and $0 < R_t <$ infinity. A grid typical of those used in the numerical turning duct calculations is shown in Fig. 4(b).

The primary independent flow variables were the jet-to-mainstream density and momentum-flux ratios. Note that the latter is equal to the ratio of jet-to-mainstream dynamic pressures, and the former is equal to the ratio of mainstream-to-jet temperatures if the jet static pressure is equal to that of the mainstream. Table 1 gives the ranges investigated for both the flow and geometric variables. Not all combinations of the independent variables in the table were tested or analyzed; only those combinations within the range given for the derived variables represent conditions that are within the range of the experiments and calculations performed.

Chronology of Previous Studies of Confined Mixing in a Rectangular Duct

From the data of Walker & Kors (1973) for mixing of a row of multiple jets in a straight duct, an empirical model was developed (Walker & Eberhardt, 1974; Holdeman & Walker, 1977) to calculate the temperature field downstream of a row of jets injected into a confined crossflow. A microcomputer program based on this empirical model was used by Holdeman (1983) to illustrate the effects of separately varying the independent flow and geometric variables and to identify the relationships among them which characterized the mixing. (Although it is recognized that a uniform temperature distribution may not always be desired, optimum is used herein (as in e.g., Holdeman & Walker, 1977; and Holdeman, Srinivasan, & Berenfeld, 1984) to identify flow and geometric conditions which lead to a uniform temperature distribution in a minimum downstream distance.)

The results of these investigations of the mixing of a single row of circular jets in a straight duct may be summarized as follows: (1) mixing improved with increasing downstream distance; (2) the momentum-flux ratio was found to be the most significant flow variable; (3) the effect of density ratio appeared to be small at constant momentum-flux ratio; (4) decreasing orifice spacing at a given momentum-flux ratio reduced penetration but increased lateral uniformity; (5) increasing orifice diameter at a constant ratio of spacing-to-diameter (S/D) increased jet penetration (y/H_0), but also decreased lateral uniformity; (6) increasing orifice diameter at a constant orifice spacing (S/H_0) increased the magnitude of the temperature difference, but jet penetration and profile shape remained similar; (7) profiles for conditions with the momentum-flux ratio (J) and orifice spacing (S/H_0) inversely coupled showed similar distributions over a range of momentum-flux ratios; (8) smaller momentum-flux ratios (and/or larger orifice spacing) required a greater downstream distance for equivalent mixing. Note from the last two items that optimum mixing was obtained for any given orifice area when the orifice spacing and momentum-flux were coupled, but that a greater downstream distance was required for equivalent mixing when either the momentum-flux ratio was small or the orifice spacing was large.

The studies by Srinivasan, Berenfeld, & Mongia (1982), Srinivasan, Coleman, & Johnson (1984), and Srinivasan, Meyers, Coleman, & White (1985) were performed to extend the available experimental data and empirical correlations on the thermal mixing of multiple jets in crossflow to include geometric and flow variations characteristic of gas turbine combustion chambers, namely variable temperature mainstream, flow area convergence, noncircular orifices, double rows of holes, and opposed rows of jets, both in-line and staggered. These experiments were an extension of those by Walker & Kors (1973).

The principal conclusions from the second tier of experiments reported in Holdeman, Srinivasan, & Berenfeld (1984) and Holdeman, Srinivasan, Coleman, Meyers, & White (1987) were: (1) the inverse relationship between the momentum-flux ratio and the orifice spacing was confirmed and quantified; (2) at constant momentum-flux ratio, variations in density ratio had only a second-order effect on the profiles; (3) flow area convergence, especially injection wall convergence,

significantly improved the mixing; (4) for orifices that were symmetric with respect to the main flow direction, the effects of shape were significant only within the first few jet diameters downstream from the injection plane; (5) penetration of slots slanted with respect to the main flow direction was less than for circular holes or slots aligned with, or perpendicular to, the main flow; (6) temperature distributions downstream from slanted slots were rotated and shifted laterally with respect to the injection centerplane; (7) jet penetration from two-dimensional (continuous) slots was similar to that downstream from closely-spaced circular holes, except that temperatures in the wake behind the jet was significantly higher for continuous slots; (8) a first-order approximation to the mixing of jets with a variable temperature mainstream was achieved by superimposing the upstream and jets-in-an-isothermal-mainstream profiles; (9) at the same momentum-flux ratio, and with the same orifice spacing (S/H_0), double rows of in-line jets had temperature distributions similar to those from a single row of circular holes of equal area at the same spacing; (10) jets from double rows of orifices of different size and spacing, or from double rows with orifices staggered, may be approximated by superimposing independent calculations of the two rows, but caution should be exercised using this model for very small offsets between the rows; (11) for opposed rows of jets, with the orifice centerlines in-line, the optimum ratio of orifice spacing to duct height is one-half of the optimum value for single-side injection at the same momentum-flux ratio; (12) for opposed rows of jets, with the orifice centerlines staggered, the optimum ratio of orifice spacing to duct height is double the optimum value for single-side injection at the same momentum-flux ratio.

In the studies by Srinivasan, Berenfeld, & Mongia (1982), Srinivasan, Coleman, & Johnson (1984), and Srinivasan, Meyers, Coleman, & White (1985) the empirical model reported by Holdeman & Walker (1977) was extended (Holdeman & Srinivasan, 1986b; Holdeman, Srinivasan, Coleman, Meyers, & White, 1987) to model the effects of a variable temperature mainstream, flow area convergence, noncircular orifices, and double rows of jets, both axially staged and opposed.

Empirical correlation of experimental data were shown (e.g., Holdeman & Srinivasan, 1986a) to provide a good predictive capability within the parameter range of the generating experiments, but empirical models must be used with caution, or not at all, outside that range. Physical modeling, in various levels of sophistication and complexity, may be used to obviate this weakness. In this regard, several one and two dimensional integral and differential jet-in-crossflow models have been developed (e.g., NASA, 1969; Karagozian, 1986) and shown to give, for example, trajectory predictions that are in good agreement with experiments. These models may provide insight into the dominant physical mechanism(s), and predict some of the characteristic parameters well, but they rarely provide enough information to completely describe the flowfield.

Although the experimental results reported by Lipshitz & Greber (1981), Riddlebaugh, Lipshitz, & Greber (1982), Lipshitz & Greber (1984) and Zizelman (1985) have provided considerable insight into the flowfield in the annular 180° curved duct that connects the exit of the combustor to the inlet of the first stage turbine in gas turbine engines using reverse-flow combustor configurations, they were not comprehensive enough to define the flow in all three coordinate directions as would be needed to extend the empirical model.

Holdeman, Reynolds, & White (1987) summarized results from the computations by Reynolds & White (1987) who used a three-dimensional, turbulent, viscous-flow computer code to investigate the effects of curvature and convergence on the mixing of single and opposed rows of dilution jets. Based on these results (Reynolds & White, 1987), the empirical model reported by Holdeman, Srinivasan, Coleman, & White (1987) for the temperature field downstream of single and multiple rows of jets injected into a straight duct was extended to model the effects of both axial and circumferential curvature with and without convergence (Srinivasan & White, 1988).

This extension of the empirical model added the capability to investigate the effects of curvature while retaining all the capabilities and limitations of the earlier versions. Also, because the empirical model calculations (for dilution jet mixing in straight ducts) shown by Holdeman & Srinivasan (1986a) were in generally better quantitative agreement with the data than three-dimensional numerical model calculations, the empirical model was extended to model the trends, but not the quantitative results, from the numerical calculations.

Flowfield Models

Empirical

The empirical model for the temperature field downstream of jets mixing with a confined crossflow is based on the observation that, for most cases of interest, vertical temperature profiles everywhere in the flowfield could be expressed in the following self-similar form (Holdeman & Walker, 1977):

$$\frac{\left(\theta - \theta^{\pm}_{min}\right)}{\left(\theta_c - \theta^{\pm}_{min}\right)} = \frac{\left(T^{\pm}_{min} - T\right)}{\left(T^{\pm}_{min} - T_c\right)} = \exp^{-\ln 2\left[\frac{y - y_c}{W^{\pm}_{1/2}}\right]^2} \qquad (2)$$

where θ is the temperature difference ratio at vertical location y, and $\theta^{\pm}_{min}$, $W^{\pm}_{\frac{1}{2}}$, θ_c, and y_c are scaling parameters as shown in Fig. 5.

Note that Fig. 5 shows injection from the top ($y/H_0 = 0$) toward an opposite wall ($y/H_0 = 1$) at the bottom. θ_c is the maximum temperature difference ratio in the vertical profile, and y_c is its location. The line defined by the locus of y_c as a function of downstream distance, x, for $z = 0$ is the thermal trajectory (centerline). Because the flow is confined, and the vertical profiles are not symmetric about the centerline, the minimum temperature difference ratios ($\theta^{\pm}_{min}$) are not zero, and they and the half-widths ($W^{\pm}_{\frac{1}{2}}$) are different for the injection (-) side ($y < y_c$) and the opposite (+) side ($y > y_c$) of the jet. Note also that Fig. 5 and Eq. (2) are the same whether the jets are hotter or cooler than the mainstream, but that $T^{\pm}_{min} > Tc \& T$ when the jets are cooler.

Correlations have been developed for each of these in terms of the independent variables J, S/D, H_0/D, z/S, and x/H_0, plus $R_{ci}H_0$ and R_t/H_0 for curved ducts and aspect ratio for noncircular orifices. These are given in the Appendix.

Numerical

The numerical code used by Reynolds & White (1987) was based on the USARTL three-dimensional model (Bruce, Mongia, & Reynolds, 1979), and used pressure and velocities as the main hydrodynamic variables. This code, or others with similar capabilities, have been used in previous validation and assessment studies reported by Srinivasan, Reynolds, Berry, Ball, Johnson, & Mongia (1983), Kenworthy, Correa, & Burrus (1983), Sturgess (1983), Mongia, Reynolds, & Srinivasan (1986), and Holdeman, Mongia, & Mularz (1988).

In the numerical model used in the studies by Srinivasan, Reynolds, Berry, Ball, Johnson, & Mongia (1983) and Reynolds & White (1987), the governing equations were represented by finite difference approximations on a staggered grid system. Hybrid differencing was used for convective terms with central differencing of all other terms. The velocity-pressure coupling used the SIMPLER algorithm (Patankar, 1980). Uniform velocities, and mass flow rates were specified at all in-flow boundaries. Standard values of the constants C_D, C_1, and C_2 were used (i.e., $C_D = 0.09$, $C_1 = 1.44$, $C_2 = 1.92$). The RMS turbulence intensity was chosen to be 7.5 percent of the local mean velocity, the inlet length scale was 2 percent of the jet diameter and the duct height for the jet and mainstream respectively, and the turbulent Prandtl Number was 0.9 for all calculations.

Results and Discussion

The following paragraphs describe the experimental results and compare them with empirical and numerical model calculations, in the context of the effects of the primary independent variables. The flow and geometry conditions corresponding to the figures shown are given in Table 1. Complete flow and geometry conditions for the cases discussed are given in Tables 2 and 3 for the experimental and numerical studies respectively. The case numbers shown correspond to those in previous reports as noted.

Single Row of Orifices

Variations with orifice size and spacing.—At constant orifice area, changes in orifice size and spacing can have a significant influence on the θ distributions. This is shown by the experimental profiles in Fig. 6 where jets from closely spaced small orifices under-penetrate and remain near the injection wall (part a), and jets from widely spaced larger orifices over-penetrate and impinge on the opposite wall (part b). In this figure, a duct cross-section is shown to the left of the data. Note that both of these configurations have the same ratio of orifice area to mainstream cross-sectional area (A_j/A_m).

The data for these conditions at $x/H_0 = 0.5$ are compared with calculated distributions in Fig. 7. The empirical model reproduces the data very well in the small orifice case, since the data are consistent with the major assumption in the empirical model that all vertical temperature distributions can be reduced to similar Gaussian profiles. The empirical model does not do as well in the larger orifice case however, as the impingement of the jets on the opposite wall results in vertical profiles which are not similar.

The numerical model calculations made with approximately 20 000 nodes, although in qualitative agreement with the data, show temperature gradients that are too steep, especially in the transverse direction. Under-prediction of the mixing was seen in the single-jet calculations by Claus (1983) also, where it was shown that the k-ε type of turbulence model underestimated the intensity. The result in Fig. 7 is typical of the numerical model calculations shown in this paper.

For the small-orifice case a coarse-grid calculation using less than 6000 nodes was also performed. The numerical results in Fig. 7 illustrate the significant influence grid selection can have on the solution obtained, and the smearing of the profiles which can occur because of numerical diffusion. Even the finer grid calculations by Srinivasan, Reynolds, Ball, Berry, & Johnson (1983) and Reynolds & White (1987) were not claimed to be grid independent; in fact, later calculations by Claus & Vanka (1990) that used over 2.4 million nodes for a single jet-in-crossflow did not appear to be grid independent. (Although the calculated coarse-grid profiles in Fig. 7 are in better quantitative agreement with the experimental data than the finer-grid solution, this result should be considered fortuitous.) In general, the finest

affordable grid should be used unless grid independence can be demonstrated.

Coupled spacing and momentum-flux ratio.—It was observed by Holdeman, Walker, & Kors (1973) that similar jet penetration was obtained over a range of momentum-flux ratios, independent of orifice diameter, when the orifice spacing and the square-root of the momentum-flux ratio were inversely proportional. This is apparent in the experimental data shown in Fig. 8 from the experiments by Srinivasan, Berenfeld, & Mongia (1982) (see also Holdeman & Walker, 1977; Holdeman, 1983; Holdeman, Srinivasan, & Berenfeld, 1984). For example, low momentum-flux ratios require large, widely spaced holes, whereas smaller closely spaced holes are appropriate for high momentum-flux ratios, as shown in Fig. 8. The duct cross-section is shown to the right of the three-dimensional oblique and isotherm contour plots for each configuration. Note that the jet penetration and the centerplane profiles are similar for all cases, but that the circumferential nonuniformity increases as the spacing increases. It follows that for low momentum-flux ratios (large spacing) a greater axial distance is required for equivalent mixing. (The experimental results in Srinivasan, Berenfeld, & Mongia (1982) suggest that circumferential nonuniformities (as in Fig. 8(a)) mix much more rapidly with increasing downstream distance than do radial nonuniformities (such as shown in Fig. 6(a)).

Generally, jet penetration and centerplane profiles are similar when the orifice spacing and the square root of the momentum-flux ratio are inversely proportional, i.e.,:

$$C = (S/H_0)\sqrt{J} \qquad (3)$$

For single-side injection, the centerplane profiles are approximately centered across the duct height and approach an isothermal distribution in the minimum downstream distance when $C = 2.5$. This appears to be independent of orifice diameter, as shown in both the calculated and experimental profiles in Fig. 9. Values of C in Eq. (3) which are a factor of two or more smaller or larger than the optimum correspond to under-penetration or over-penetration respectively (see Figs. 6 and 7 and Table 1). A summary of the spacing and momentum-flux ratio relationships for single-side injection is given in Table 4.

Flow area convergence.—The effect of flow area convergence on the temperature profiles for $S/H_0 = 0.5$ and $H_0/D = 4$ with $J = 26$ is shown in Fig. 10. The profiles in Fig. 10(a) are from the straight duct, whereas those in Figs. 10(b) and (c) are for test sections that converge symmetrically and asymmetrically, respectively, to one-half of the injection plane height, H_0, in a downstream distance equal to H_0 (i.e., $dH/dx = 0.5$). Note that the ordinate in these figures is nondimensionalized by the local height of the duct, so the gradients are less steep than they would be in physical space.

At all downstream locations, the profiles for symmetric convergence (Fig. 10(b)) are more uniform than the corresponding straight duct profiles. An even greater effect was observed when all of the turning was on the injection wall. These profiles (Fig. 10(c)) are much more uniform in both the transverse and lateral directions. Although detailed analysis was not undertaken, Holdeman, Srinivasan, and Berenfeld (1984) hypothesized that enhanced mixing in converging sections could result from the stretching of the strong dual-vortex field typical of a jet-in-crossflow (c.f. also Stevens & Carrotte, 1988).

Square holes.—A single test was performed by Srinivasan, Coleman, & Johnson (1984) with the conventional circular holes replaced with square holes to identify the effect of this change in orifice shape on the mixing. Square orifices were chosen to represent the approximation often made in multi-dimensional numerical modeling due to limitations on the number of grid nodes available. Figure 11 compares three-dimensional oblique plots of the temperature distribution for equal-area square and round holes with $S/H_0 = 1$ and $H_0/D = 4$ at intermediate momentum-flux ratios (slightly less than 25). The mean temperature distributions are nearly identical at all downstream locations.

Slots and holes.—Figure 12 shows three-dimensional oblique θ distributions for equally spaced equivalent-area streamlined, bluff, and slanted slots with $S/H_0 = 0.5$ and $H_0/D = 4$. These slots had an aspect ratio (length/width) of 2.8, with their major axes aligned with, perpendicular to, and slanted at 45° to the mainstream flow direction. All profiles comparison shown in this figure are for intermediate momentum-flux ratios.

The streamlined slots (Fig.12(a)) have deeper jet penetration compared to the equal-area circular holes shown in Fig. 2. Figure 12(b) shows that, for $x/H_0 < 1$, jets from bluff slots are more two-dimensional across the orifice centerplane, and their penetration is slightly less than for streamlined slots or round holes. Farther downstream, both of the slot configurations, and the circular holes give very similar mixed temperature distributions.

Figure 12(c) shows the temperature distribution that results when the same slot is slanted at 45° to the mainflow direction. The three-dimensional figures suggest that the asymmetry of the orifices with respect to the main flow direction promotes the development of one vortex of the pair, but suppresses the other. The penetration of the jets is noticeably reduced for this case, and the mixing does not appear to be any better. Thus, there does not seem to be any advantage to this configuration in a rectangular duct, at least at the optimum orifice spacing and momentum-flux ratio relationship for round holes.

Further insight into the mixing in this case is provided by the isotherm contours in Fig. 13(a) for circular holes and in Fig. 13(b) for the 45° slanted slots. Note that at the closest location ($x/H_0 = 0.25$) the isotherms for the flow from the slanted slots are inclined compared to those for jets from circular holes. The influence of the adjacent image vorticies in this flow would be to laterally shift the jet centerplanes with increasing downstream distance, as can be observed in both Figs. 12(c) and 13(b). Comparing the contours at $x/H_0 = 0.5$ to those at $x/H_0 = 0.25$ suggests that the distribution has rotated farther as well as shifted. This also supports the observation made from the oblique plots that the vorticies appeared to be of unequal strength.

Figure 14 shows experimental and calculated three-dimensional oblique θ distributions for slanted slots at intermediate momentum-flux ratios. The empirical model calculations include a modification to account for the observed centerplane shift, but do not model the asymmetry (Holdeman, Srinivasan, Coleman, Meyers, & White, 1987). In contrast to this, both the translation and rotation of the mixing pattern are apparent in the numerical calculations, although the gradients in these appear to be too steep as are those in almost all of the numerical calculations shown herein.

In the same study, a limited number of tests were performed with two-dimensional slots in place of the row of discreet orifices. Figures 15(a) and 16(a) show the results for, respectively, a wide continuous slot ($A_j/A_m = 0.1$) at a low momentum-flux ratio ($J = 6.7$) and a narrow continuous slot ($A_j/A_m = 0.05$) at a high momentum-flux ratio ($J = 105.4$). Distributions for closely spaced ($S/D = 2$) circular holes are shown in Figs. 15(b) and 16(b), and centerplane profiles for the circular and continuous slot jets are shown in Figs. 15(c) and 16(c). The similarity in the penetration shown by these profiles is surprising, since the two-dimensional slot flow completely blocks the mainflow, whereas the discreet jet flow is highly three-dimensional. In the latter case the mainstream flow is deflected around, as well as over, the jets, creating the well known vortex pair and kidney shaped mixing pattern. The increased blockage in the slot-jet cases result in less mixing and higher temperatures in the wake region of these flows compared to equal-area closely-spaced holes.

Experimental profiles for the narrow slot at intermediate momentum-flux ratios are similar to those shown in Fig. 15(a) for the wide slot at a low momentum-flux ratio, and profiles for the wide slot at an intermediate momentum-flux ratio are similar to those shown in Fig. 16(a) for the narrow slot at a high momentum-flux ratio (Srinivasan, Coleman, & Johnson, 1984). The corresponding circular hole cases are also similar, as expected since the corresponding values of $C = (S/H_0)\sqrt{(J)}$ are also similar.

Density ratio.—It was suggested by Holdeman, Walker, & Kors (1973) that the density ratio did not need to be considered independently from the momentum-flux ratio. This was confirmed over a broader range of density ratios in the experiments by Srinivasan, Berenfeld, & Mongia (1982). The results from these experiments in Figs. 17 and 18 show the effect of the density ratio on the θ distributions for (nearly) matched jet-to-mainstream velocity, mass-flux, and momentum-flux ratios. The profiles in Fig. 17 are for an orifice configuration with $S/H_0 = 0.5$ and $H_0/D = 8$ (plate A in Fig. 3) for three different flow conditions. For each of these, profiles are shown at downstream distances of $x/H_0 = 0.5$, 1, and 2 from left to right. The profiles in Fig. 17(a) are for hot jets and an ambient temperature mainstream, whereas those in parts b and c are for ambient jets and a heated mainstream.

In Figs. 17(a) and (b) the momentum-flux ratios are nearly equal and the profiles are quite similar although the density ratio is 0.65 in Fig. 17(a) and 2.2 in Fig. 17(b). The slightly smaller θ levels in 17(a) result from the smaller jet-to-mainstream mass flow ratio in the case of hot jets. In contrast, the profiles in Fig. 17(c) show over-penetration, which appears to be the result of an almost quadrupled ratio of the jet-to-mainstream momentum-flux. Note, however, that the jet-to-mainstream velocity ratios, R, are about the same for the hot-jets and ambient mainstream case shown in 17(a), and the ambient jets and hot mainstream case in 17(c).

Figure 18 shows a similar comparison for an orifice plate with the same ratios of orifice spacing to duct height (S/H_0) but with larger holes. The hot jets and ambient mainstream case and ambient jets and hot mainstream case in Figs. 18(a) and (b), respectively have nearly equal jet-to-mainstream mass-flux ratios, M, but note that the jets in Fig. 18(b) do not penetrate nearly as far into the mainstream apparently as a result of their lower momentum-flux ratio. The experimental profiles for a case with a heated mainstream flow, but with a slightly smaller momentum-flux ratio than that for the hot jets case in Fig. 18(a), is shown in Fig. 10(a) here and in Fig. 5(b) in paper AIAA-90-1201 (see Holdeman, Srinivasan, and Berenfeld, 1984).

Variable temperature mainstream.—The influence of a nonisothermal mainstream flow on the profiles for intermediate momentum-flux ratios with $S/H_0 = 0.5$, $H_0/D = 4$ is shown in Fig. 19. The isothermal mainstream case is shown in the top row. In the center row in the figure, the upstream profile (left frame) is coldest near the injection wall, whereas in the bottom row, the upstream profile (left frame) is coldest near the opposite wall. In this figure, the hottest temperature in the mainstream for each case was used as T_m in the definition of θ.

Experimental, empirical, and numerical results for the top-cold case are shown in Fig. 20. The empirical calculations are from a superposition of the upstream profile and the corresponding jets-in-an-isothermal mainstream distribution (Holdeman, Srinivasan, & Berenfeld, 1984). Although this gives a good first-order approximation, it should be noted that with a variable temperature mainstream there can be cross-stream thermal transport because of the flow of mainstream fluid around the jets (and hence to different y locations), and this is not accounted for in superimposing the distributions. This becomes apparent if the local mainstream temperature, $T_m(y)$, is used in the definition of θ in Eq. (1).

In the variable temperature mainstream case the numerical model results agree well with the experimental data, especially on the jet centerplane, but the transverse mixing is under-predicted, as in the corresponding isothermal mainstream case shown in Fig. 9(b).

Double Rows of Holes

Figure 21 shows three-dimensional oblique and isotherm contour plots at $x/H_0 = 0.5$ for a single row of round holes and several equal-area double-row circular hole configurations at intermediate momentum-flux ratios. The single row (configuration C in Fig. 3) is shown in Fig. 21(a); flow downstream from two rows of orifices with centerlines aligned (configuration M) is shown in Fig. 21(b); two rows of jets with a different hole diameter and spacing in each row (configuration N) are shown in 21(c); and a staggered double-row (configuration O) is shown in Fig. 21(d). For the double row configurations, $x/H_0 = 0$ was midway between the rows.

Figure 22 shows both experimental and calculated temperature distributions for a double row of in-line holes ($S_x/H_0 = 0.5$). It was observed from the experimental profiles in Holdeman, Srinivasan, Coleman, Meyers, & White (1987) that the two configurations have very similar temperature distributions, and this is seen in the calculated profiles as well. In this case the empirical model calculations are derived by superimposing the distributions from the two rows.

Both experimental and calculated temperature distributions are shown in Fig. 23 for a double-row configuration with $S_x/H_0 = 0.25$ where the trailing row has twice as many orifices as the lead row. Note that the orifice area is the same for both rows. The similarity in the profiles shows the dominance of the lead row in establishing the jet penetration and first-order profile shape (Holdeman, Srinivasan, Coleman, Meyers, & White, 1987). The same conclusion is supported by the empirical and numerical calculations. As with the double row of in-line holes, the empirical calculations for this case were obtained by superimposing separate calculations for the two rows.

The influence of the leading row on the temperature distributions is evident in Fig. 21(d) also, where distributions from a double row of staggered jets ($S_x/H_0 = 0.5$) is shown for comparison with the other configurations. The jets from the leading row penetrate farther across the duct than do those from the single row, as would be expected due to their larger spacing, but the penetration of the jets from the trailing row is suppressed, probably by the vortex field from the leading row. Farther downstream this distribution was similar to that from a single row at one-half the spacing of the lead row. This flow was modeled empirically by superimposing separate calculations of each row, but note that this approach significantly overestimates the jet penetration for very small axial distances, S_x/H_0, between the rows (see Holdeman & Srinivasan, 1986b).

Opposing Rows of Jets

The next three sections show results for two-side injection from opposing rows of jets, with: (1) the jet centerlines on top and bottom directly opposite each other; and (2) the jet centerlines on top and bottom staggered in the z (circumferential) direction. The experimental results are shown and compared with the single-side results in Figs. 24 and 26. In these figures, a duct cross-section is shown to scale to the left of the data.

Opposed rows of in-line jets.—Figure 24 shows a comparison between single-side and opposed jet injection cases for intermediate momentum-flux ratios. For these momentum-flux ratios, an appropriate orifice spacing to duct height ratio for optimum single-side mixing is approximately 0.5 (see Eq. (3)), as confirmed by the profiles in Fig. 8.

For opposed jet injection, with equal momentum-flux ratios on both sides, the effective mixing height is half the duct height, based on the result in Kamotani & Greber (1974) that the effect of an opposite wall is similar to that of the plane of symmetry in an opposed jet configuration (c.f. also Wittig, Elbahar, & Noll, 1984).

Thus the appropriate orifice spacing to duct height ratio for opposed jet injection at these intermediate momentum-flux ratios would be about $S/H_0 = 0.25$. Dimensionless temperature distributions downstream of jets with this spacing are shown in the bottom row of Fig. 24; and the two streams do indeed mix very rapidly. Note that since the orifices in Figs. 24(a) and (b) are the same size, the jet to mainstream flow ratio is four times greater in the opposed jet case than in the single-side case. If it is desired to maintain an equal flow rate, the orifice diameter must be halved, since there is injection from both sides, and the opposed jet cases require twice as many holes in the row compared to the optimum single-side case.

Experimental and calculated profiles for opposed rows of jets of identical orifice spacing and diameter, with the orifice centerlines in-line are shown in Fig. 25. The empirical model predicts the opposed-jet case very well, as the experimental profiles on both sides of the plane of symmetry support the Gaussian profile assumption. The numerical model results show the steep transverse and lateral gradients indicative of too little mixing, as seen in almost all of the previous calculations also, but the jet penetration is in good agreement with the data.

Opposed rows of staggered jets.—Figure 26 shows comparisons between single-side and staggered jet injection for intermediate momentum-flux ratios. Since for opposed in-line injection, it was found that the effective mixing height was half of the duct height, it was hypothesized that for staggered jets the effective orifice spacing would be half the actual spacing.

This hypothesis is verified by the rapid mixing of the two streams in the bottom row of profiles in Fig. 26. In this figure, the orifice spacing for the jets on each side is twice the optimum value for one-side injection at the given momentum-flux ratio. That is, a configuration that mixes well with one-side injection mixes even faster when every other orifice is moved to the opposite wall (see the duct schematic to the left of the data in Fig. 26).

Empirical and numerical model calculations for an opposed row of staggered jets are compared with the data in Fig. 27. The empirical model does not handle this complex case well, as the fluid dynamic interactions here are not amenable to a direct extension of the Gaussian profile and superposition type of modeling appropriate for most of the single-side and opposed-jet cases of interest. The numerical model calculations are not in appreciably better agreement with the data than the empirical model results however, as the mixing is under-predicted here as in the previous cases. More recent calculations for an opposed row of staggered jets are given by Smith (1990).

A summary of the spacing and momentum-flux ratio relationships which give optimum mixing for opposed in-line and staggered jets is given in Table 4.

Opposed rows of jets from slanted slots.—Numerical model calculations for 2.8:1 aspect ratio slots slanted at 45° to the direction of the mainstream flow are shown in Fig. 28 for opposed row/in-line jet configurations in a straight duct.

In opposed-jet/slanted-slot configurations, the slots on opposite sides of the duct may be slanted in either the same or opposite directions. If aligned, the result is similar to single-side injection toward an opposite wall (as was observed previously for circular holes). Centerplane and cross-stream contour plots for this case are shown in Figs. 28(a), (d), and (e), and may be compared to the corresponding plots for circular holes in Figs. 28(c), (h), and (i). The aligned slot configuration imparts a translation to the flow consistent with the experimental results (Srinivasan, Meyers, Coleman, & White, 1985). It was also reported therein that for the momentum-flux ratios tested, this configuration results in augmentation of one of the vorticies of the normal vortex pair, and suppression of the other, and the jets mix less rapidly than in the circular hole configuration. This is also evident in the calculations shown in Figs. 28(a), (d), and (e).

If the slots on opposite sides of the duct are crossed, the jet flow shifts in opposite directions in the two halves of the duct, with opposite transverse velocities imparted on the top and bottom creating the potential for large scale vortex interaction and high shear between the halves. However, the centerplane and cross-stream contours for an opposed row of crossed slots shown in Figs. 28(b), (f), and (g), at what is an optimum spacing for round holes, do not suggest any improvement in the mixing over the corresponding circular hole case. Thus, it was concluded by Holdeman, Reynolds, and White (1987) that there does not seem to be any advantage to this configuration, at least at the optimum ratio between orifice spacing and momentum-flux ratio for round holes.

Effects of Curvature and Convergence

Differences between ID and OD injection into a curved duct.—Figures 29 and 30 show centerplane and cross-stream temperature distributions calculated with the numerical and empirical models respectively for the flowfield downstream of a row of jets injected from the inner (ID) and outer (OD) walls into a uniform mainstream flow in a nonconverging duct. Orifice configuration C in Fig. 3 ($S/H_0 = 0.5$; $H_0/D = 4$) with $C_d = 0.64$ was used for these calculations with the jet-to-mainstream momentum-flux ratio, J, equal to 26.4. This is an appropriate combination of orifice spacing and momentum-flux ratio for optimum mixing in a straight duct. For comparison with the turning duct cases, contours calculated for a straight duct with the same jet flow and orifice geometry are also shown in parts (b), (c), (f), and (g) of these figures. The cross-stream plots for the straight duct case are shown at downstream distances equal to the distance along the injection wall at 30° into the turn for ID and OD injection, respectively.

Comparison of the centerplane view of injection from the ID wall in a curved duct with that in a straight channel, parts a and b, shows that the penetration is similar. Examination of the cross stream plots in parts e and f, however, shows that for ID injection into the curved duct the familiar kidney shape is not evident; i.e., for ID injection the minimum temperature at any radius is on the centerplane ($z/S = 0$), whereas for OD injection and straight-duct flows the minimum temperature is often off the centerplane.

Parts c and d, and g and h show a comparison of OD injection upstream of a 180 turn with injection into a straight duct (parts c and g are from the same straight duct calculation shown in parts b and f, with the plots inverted to facilitate comparison with the OD injection case). For OD injection, the penetration and mixing are similar to that in a straight duct.

Parts e and h in Figs. 29 and 30 show that the jet structure and mixing are significantly different for the ID and OD jets. Note also that the jet trajectories drift slightly toward the ID wall of the turn compared to where they would be in a straight duct. This latter result was observed in the experimental results in Lipshitz & Greber (1984).

Opposed rows with jet centerlines staggered.—It was reported in Holdeman, Srinivasan, & Berenfeld (1984) and Holdeman & Srinivasan (1986a) that enhanced mixing was obtained when alternate jets for optimum one-side injection were moved to the opposite wall, creating opposed rows of jets with centerlines staggered. For example, if configuration C is selected to optimize the mixing for one side injection, then configurations G and H would be appropriate choices for opposite sides of the duct in an opposed row/staggered jet configuration. Jet centerline and cross-stream contour plots for the analogous opposed row configuration in a turning duct is shown in Figs. 31 and 32. Note that parts b and c show planes through the OD and ID jets, respectively. Corresponding plots for separate rows of OD and ID jets are shown in parts a and e, and d and g, respectively.

The contours for opposed rows of staggered jets in a turning duct (Figs. 31 and 32) show that both the OD and ID jets in this configuration penetrate farther than the comparable single-side case. This was also seen in the straight duct experiments. A difference between the cross-stream shape of the distributions downstream from OD and ID jets is apparent also, and is consistent with the corresponding contours of the separate OD and ID jet configurations.

Opposed rows with jet centerlines in-line.—An alternative to staggered centerlines in the opposed row configuration is to have the centerlines directly opposed. To maintain the appropriate ratio of orifice spacing to mixing height for this case, the orifice spacing must be halved since the effective mixing height is half the height of the duct (Holdeman, Srinivasan, & Berenfeld, 1984; Wittig, Elbahar, & Noll, 1984). Since there will be four times as many injection locations for opposed/in-line injection, the orifice diameters must be half of that for the single-side case if the same mass flow split is desired. This is shown in configuration L ($S/H_0 = 0.25$, $H_0/D = 8$) in Fig. 3. Centerplane and cross-stream contour plots for this configuration with $J = 26.4$ are shown in parts a and c of Figs. 33 and 34 for calculations made with the numerical and empirical models, respectively.

A lower jet-to-mainstream momentum-flux ratio requires a larger orifice spacing to maintain optimum mixing (and larger orifices will probably also be needed to give the required total orifice area). Centerplane and cross-stream temperature contours for configuration C with $J = 6.6$ for opposed rows of in-line jets are shown in parts b and d of Figs. 33 and 34. The similarity of the flow pattern is evident in both the numerical and empirical model calculations when the momentum-flux ratio and the square of the orifice spacing are inversely proportional. Compare parts b and d for $J = 6.6$ and $S/H_0 = 0.5$ to parts a and c for $J = 26.4$ and $S/H_0 = 0.25$, and note that $C = 1.28$ for both of these. This similarity was also seen in the experimental and analytical results for opposed rows of in-line jets injected into a straight duct.

Effects of radius of curvature in the x-r plane.—The effect of varying the radius of curvature, R_{ci}, is shown in Figs. 35 and 36 for calculations made with the numerical and empirical models, respectively. Parts b and e are centerplane and cross-stream contours for an ID radius of curvature equal to one-fourth the height of the inlet duct, i.e., $R_{ci}/H_0 = 0.25$. The jet-to-mainstream momentum-flux ratio is 6.6 with an opposed row/in-line jets configuration with $S/H_0 = 0.5$ and $H_0/D = 4$ (configuration C). Both the centerplane and cross-stream distributions for these and the larger radius of curvature ($R_{ci}/H_0 = 0.5$) shown in Figs. 33 and 34 are similar. For comparison, centerplane and cross-stream contour plots for the comparable straight duct case are shown in parts a, c, and d. As in previous figures the straight and turning duct flows are similar, but the difference between the mixing of the ID and OD jets is evident in the turning duct cases.

Mixing of jets in an annular duct (effects of curvature in the r-z plane).—Calculated centerplane and cross-stream contours for a straight annulus and a comparable rectangular duct are shown in Figs. 37 and 38 for numerical and empirical models, respectively. Cross-section contours, for both the annular and rectangular ducts, are shown at a downstream distance of $x/H_0 = 0.75$ for the numerical model calculation.

For the annular duct, the inside radius (ID) of the annulus was equal to the duct height, i.e., $R_i/H_0 = 1$. The orifice geometry was again an opposed row/in-line jets (configuration C) with $J = 6.6$. Similar penetration and mixing, as seen in both the centerplane and cross-stream contours, was achieved by specifying the jet spacing for the annular duct to be equal to that in the rectangular duct at the radius which divides the annulus into equal areas ($r - R_{ci} = H_0/\sqrt{(2)}$).

Convergence effects.—The effect of a 1:3 (exit:inlet) area ratio convergence in turning ducts is shown in the centerplane and cross-stream contours in Figs. 39 and 40 for the opposed row/in-line jets configuration. For a turning duct, this convergence may be obtained through reduction in the duct height or by circumferential convergence if the exit annulus is at a

smaller radius (closer to the engine centerline) than the inlet. Centerplane and cross-stream temperature contours for these turning and converging cases are shown in parts b and f, and c and g, respectively. Temperature distributions, especially the cross-stream contours, are similar for both radial and circumferential convergence. Centerplane and cross-stream plots for a straight converging duct are shown in parts a, d, and e.

Jets injected into a can.—This is the limiting case for OD injection with curvature in the r-z plane where the radius of the inner annulus is equal to zero. Calculated temperature contours for jet injection into a section of a can are shown in Figs. 41 and 42. Cross-stream contours are shown at a downstream distances of $x/H_0 = 0.75$ for the numerical model, and at downstream distances of $x/H_0 = 0.25$ and 0.75 for the empirical model. The corresponding centerplane and cross-stream contours for the rectangular duct case are shown in Figs. 29 and 30.

The jet-to-mainstream momentum-flux ratio was 26.4. The jet spacing for this case was specified, at the radius which divides the can into equal areas, as that appropriate for injection of a row of jets into a rectangular duct. That is, the relationship of the spacing between jet centerlines to the number of holes around the circumference of the can would be

$$S = 2\pi R_{1/2}/n \tag{4}$$

where

$$R_{1/2} = H_0/\left(\sqrt{2}\right) \tag{5}$$

Substituting these into the spacing and momentum-flux relationship for a rectangular duct (Eq. (3)) gives the appropriate number of holes as

$$n = \pi\sqrt{2J}/C \tag{6}$$

It follows that each sector would be 360/n°.

Applicability and Limitations

These results suggest that for a given momentum-flux ratio and downstream distance, combustor design procedure should first identify the circumferential orifice spacing (S/H_0) required to obtain the desired penetration and profile shape. The orifice size would then be chosen to provide the required jet-to-mainstream mass flow ratio. Because the penetration varies slightly with orifice size and shape, and other parameters such as the combustor pressure loss and the ratio of the orifice spacing to diameter (S/D) must be monitored to insure that the suggested configuration is physically realistic, some adjustments, including noncircular orifices or multiple rows, may be needed to arrive at the final design.

Empirical

Examination of the empirical model results shown here suggest that correlation of experimental data can provide a good predictive capability within the parameter range of the generating experiments, provided that the experimental results are consistent with the assumptions made in the empirical model. These models must, however, be used with caution, or not at all, outside this range.

The range of the experiments on which the empirical model used in this study was based are given in Table 1. The density ratio, momentum-flux ratio, orifice spacing, and orifice size were the primary independent variables. The orifice-to-mainstream area ratio, the jet-to-total mass flow split, and the constant of proportionality between the orifice spacing and momentum-flux ratio, which are derived from the primary variables are also given in the table. Not all combinations of the independent variables in the table were tested; only those combinations which are within the range given for the derived variables represent conditions that are within the range of the experiments and calculations.

Examining the results in Figs. 6 to 42 in the context of Eq. (3) suggests that generally the empirical model would be expected to provide good temperature field predictions for single-side injection when $1 < C < 5$. Similarly, good predictions would be expected for opposed in-line jets provided that $0.5 < C < 2.5$. This model does not work well for impinging flows as the experimental temperature distributions are not consistent with the assumption of Gaussian profile similarity in the empirical model. The experimental profiles for conditions giving optimum mixing in opposed staggered-jet configurations are also somewhat at variance with the model assumptions, and the satisfactory agreement with the data in these cases must be considered fortuitous.

Use of the empirical model in regions close to the injection location ($x/D < 1$) is not recommended. Also, a major weakness of the empirical model used here (Holdeman, Srinivasan, and White, 1988) and previous versions is that the form of the empirical correlations precludes their use for semi-confined flows (large H_0/D or S/D), single jet flows, or flows in which it is known a priori that the primary assumptions in the model will be invalid.

Numerical

It is significant to note that the numerical model is not subject to the inherent limitation of the empirical model regarding profile shape and confinement. Thus, three-dimensional codes can provide calculations for complex flows for which the assumptions in the empirical model are known to be invalid, or that are outside the range of available experiments. Furthermore numerical models provide calculations for all flowfield parameters of interest, not just those that happen to have been empirically correlated.

The numerical calculations correctly show the trends which result from variation of the independent flow and geometric

variables, although the results consistently exhibit too little mixing, consistent with previous jet-in-crossflow calculations using a k-ε model reported in Claus (1983). The numerical model calculations for the slanted slots and staggered jet cases are encouraging in that the experimental data for these cases show profiles that are not consistent with the primary assumptions in the empirical model.

The numerical calculations performed were shown to be grid sensitive, and false diffusion was known to be present. Uncertainties also exist in these calculations regarding the validity of turbulence model assumptions, and due to unmeasured (and hence assumed) boundary conditions. The results shown here are not intended to represent the agreement possible from numerical models at this time, as better temperature field agreement could undoubtedly have been achieved by adjusting model constants and/or inlet boundary conditions. Since this was not necessary to satisfy the objective of evaluating the potential of these codes vis-a-vis combustor dilution zone flowfields, and because the mean temperature was the only parameter compared, no adjustments were made.

Thus, consistent with previous assessments, three-dimensional calculations of complex flows (circa 1985), such as those shown herein, should be considered as only qualitatively accurate, but are useful in guiding design changes or in perturbation analyses. Although these codes were deemed sufficiently promising to justify further development and assessment, they possessed neither sufficient accuracy nor efficiency for practical use as a general engineering tool. Recent codes with improved numerics, accuracy, and turbulence models offer more quantitative predictions, but there would appear to be a continuing need for the empirical model as a near-term design tool, provided that the conditions of interest are within the range of the experience on which the model is based.

Summary of Results

The principal conclusions from the experimental results summarized herein are:

1. Variations in momentum-flux ratio and orifice size and spacing have a significant effect on the flow distribution.

2. Similar distributions can be obtained, independent of orifice diameter, when the orifice spacing is inversely proportional to the square-root of the momentum-flux ratio.

3. Flow area convergence, especially injection wall convergence, significantly improves the mixing.

4. For orifices that are symmetric with respect to the main flow direction, the effects of shape are significant only in the region near the injection plane. Beyond $x/H_0 = 1$ ($x/D > 4$ for the orifices tested) temperature distributions were similar to those observed from equally spaced equal-area circular orifices.

5. The penetration and mixing of 45° slanted slots are less than for streamlined, bluff or equivalent-area circular holes. Also, temperature distributions for slanted slots are rotated and shift laterally with respect to the injection centerplane.

6. Jet penetration for two-dimensional slots is similar to the centerplane value for closely-spaced ($S/D = 2$) holes, but the temperature difference ratios show that the mixing is significantly slower for two-dimensional slots.

7. A first-order approximation to the mixing of jets with a variable temperature mainstream can be achieved by superimposing the jets-in-an-isothermal-mainstream and upstream profiles.

8. With the same orifice spacing in (at least) the lead row, double rows of jets have temperature distributions similar to those from a single row of equally-spaced, equivalent-area circular orifices.

9. For opposed rows of jets, with the orifice centerlines in-line, the optimum ratio of orifice spacing to duct height is one-half of the optimum value for single-side injection at the same momentum-flux ratio. Similar mixing was observed to that from comparable single-side cases, except that better mixing was observed at the same downstream distance for opposed jets because the effective mixing height is less than the channel height for this case.

10. For opposed rows of jets, with the orifice centerlines staggered, the optimum ratio of orifice spacing to duct height is double the optimum value for single-side injection at the same momentum-flux ratio. This configuration exhibited even better mixing than optimum single side injection. That is, a configuration that mixes well with one-side injection performs even better when every other orifice is moved to the opposite wall.

Temperature field measurements from the experiments cited above are compared with distributions calculated with an empirical model based on assumed vertical profile similarity and superposition, and with calculations made with a three-dimensional elliptic code using a standard k-ε turbulence model. The results can be summarized as follows:

Empirical model calculations provide very good results for modeled parameters within the range of experiments whenever the primary assumptions in the model are satisfied.

Numerical model calculations can predict all flowfield quantities, flows outside the range of experiments, or flows where empirical assumptions are invalid. Three-dimensional

code calculations made in this study correctly approximate the trends which result from variation of the independent flow and geometric variables, but they consistently exhibit too little mixing. Numerical calculations should yield more quantitative predictions with improvements in numerics, accuracy, and turbulence models.

An existing empirical model for the temperature field downstream of single and multiple rows of jets injected into a confined crossflow has been extended to model the effects of curvature and convergence on the mixing. This extension is based on the results of a numerical study of these effects using a three-dimensional turbulent flow computer code. Temperature distributions calculated with both the numerical and empirical models show the effects of flow area convergence, radius of curvature, and inner and outer wall injection for single and opposed rows of jets.

The following conclusions can be made from the computational study:

1. Jet penetration and mixing in a turning and converging duct are similar to the effects seen in a converging straight channel, namely that the optimum orifice spacing and momentum-flux relationships are unchanged, and the mixing is not inhibited by the convergence. This appears to be independent of whether the convergence in the turning duct is radial or circumferential.

2. Curvature in the mainflow direction causes a drift of the jet trajectories toward the inner wall. The different structure for the ID and OD jets, observed in the calculations with the numerical model, are shown in calculations with the empirical model also.

3. Jet trajectories in an annulus (or can) are similar to those in a rectangular duct for the same jet-to-mainstream momentum-flux and orifice-spacing-to-duct-height (radius) ratios when the spacing is specified at the radius dividing the annulus (or can) into equal areas.

Appendix—Correlation Equations

Jet Thermal CenterlineTrajectory

$$y_c/H_{eq} = (a_1)(0.3575)(J)^{0.25}(S/D)^{0.14}(H_{eq}/D)^{-0.45}(C_d)^{0.155} \times (x/H_{eq})^{0.17}(\exp(-b))$$

where

$$a_1 = \min[(1 + S/H_{eq}),2]$$

and

$$b = (0.091)(x/H_{eq})^2[(H_{eq}/S) - (J^{0.5})/3.5]$$

Centerplane Maximum Temperature Difference Ratio

$$\theta_c = \theta_{EB} + (1 - \theta_{EB})\left[(a_1)(J)^{-0.35}(C_d)^{0.5}(H_{eq}/D)^{-1} \times (x/H_{eq})^{-1}\right]^f$$

where

$$f = 1.15[(S/H_{eq})/(1 + S/H_{eq})]^{0.5}$$

and

$$\theta_{EB} = w_j/w_T$$

Centerplane Minimum Temperature Difference Ratios

$$(\theta^+_{min})/(\theta_c) = 1 - \exp(-c^+)$$

where

$$c^+ = (a_3)(0.038)(J)^{1.62}(S/D)^{1.5}(H_{eq}/D)^{-2.57}(C_d)^{0.535} \times (x/H_{eq})^{1.1}$$

and

$$a_3 = 1 \text{ if } (Y_c/H_{eq} + W^+_{1/2}/H_{eq}) \le 1$$

$$= (H_0/H_{eq})^{3.67} \text{ if } (Y_c/H_{eq} + W^+_{1/2}/H_{eq}) > 1$$

$$(\theta^-_{min})/(\theta_c) = 1 - \exp(-c^-)$$

where

$$c^- = (Q)(a_4)(J)^{-0.3}(S/D)^{-1.4}(H_{eq}/D)^{0.9}(C_d)^{0.25}(x/H_{eq})^{0.9}$$

and

$a_4 = 1.57$ if R_{ci}/H_{eq} = infinity (straight duct)

$= 3.93$ if R_{ci}/H_{eq} < infinity (curved duct)

$Q = 1$ if $\left(Y_c/H_{eq} + W^+_{½}/H_{eq}\right) \le 1$ or R_{ci}/H_{eq} < infinity

$= \exp\left[(0.22)(x/H_{eq})^2\left((J^{0.5})/5 - S/H_{eq}\right)\right]$ if $\left(y_c/H_{eq} + W^+_{½}/H_{eq}\right) > 1$

R_{ci}/H_{eq} = infinity

Centerplane Half-Widths

$$\left(W^+_{½}\right)/H_{eq} = (a_5)(J)^{0.18}(S/D)^{-0.25}\left(H_0/H_{eq}\right)^{0.5}(C_d)^{0.125} \times \left(x/H_{eq}\right)^{0.5}$$

where

$a_5 = 0.1623$ if R_{ci}/H_{eq} = infinity (straight duct)

$= 0.3$ if R_{ci}/H_{eq} < infinity (curved duct)

$$\left(W^-_{½}\right)/H_{eq} = (a_6)(J)^{0.15}(S/D)^{0.27}\left(H_{eq}/D\right)^{-0.38}\left(H_0/H_{eq}\right)^{0.5} \times (C_d)^{0.055}\left(x/H_{eq}\right)^{0.12}$$

where

$a_6 = 0.2$ if R_{ci}/H_{eq} = infinity (straight duct)

$= 0.5$ if R_{ci}/H_{eq} < infinity (curved duct)

Off-centerplane Thermal Trajectory

$$y_{c,z}/y_c = 1 - (4)(z/S)^2(\exp(-g))$$

where

$$g = (0.227)(J)^{0.67}(S/D)^{-1}\left(H_{eq}/D\right)^{0.54}(C_d)^{0.23}\left(x/H_{eq}\right)^{0.54}$$

Off-centerplane Maximum Temperature Difference Ratio

$$\left(\theta_{c,z}\right)/\theta_c = 1 - (4)(z/S)^2(\exp(-d))$$

where

$$d = (0.452)(J)^{0.53}(S/D)^{-1.53}\left(H_{eq}/D\right)^{0.83}(C_d)^{0.35}\left(x/H_{eq}\right)^{0.83}$$

Off-centerplane Minimum Temperature Difference Ratios

$$\left(\theta^{\pm}_{min,z}\right)/\left(\theta_{c,z}\right) = \left(\theta^{\pm}_{min}\right)/(\theta_c)$$

Off-centerplane Half-widths

$$\left(W^{\pm}_{½,z}\right)/H_{eq} = \left(W^{\pm}_{½}\right)/H_{eq}$$

The six scaling parameters, y_c/H_{eq}, θ_c, θ^+_{min}, θ^-_{min}, $W^+_{½}/H_{eq}$, and $W^-_{½}/H_{eq}$, are used in Eq. (2) to define the vertical profile at any x,z location in the flow. For all except the case of opposed rows of jets with centerlines in-line, H_{eq} in the correlation equations is equal to H_0, the height of the duct at the injection location.

Nonisothermal Mainstream
Double (axially staged) Rows of Jets
Opposed Rows of Jets with Centerlines Staggered

It was shown by Holdeman and Srinivasan (1986a) that these flows can be satisfactorily modeled by superimposing independent calculations of the separate elements. This is accomplished as follows:

$$\theta = \left[\theta_1 + \theta_2 - (2)(\theta_1)(\theta_2)\right]/\left[1 - (\theta_1)(\theta_2)\right]$$

Note that $\theta = \theta_1$ at any location where $\theta_2 = 0$ (and $\theta = \theta_2$ if $\theta_1 = 0$); and that $\theta \le 1$ (provided that θ_1 and θ_2 are each ≤ 1). Also, for the completely mixed case θ_{EB} is equal to the ratio of the jet flow to the total flow as required.

Opposed Rows of Jets with Centerlines In-line

It was observed by Kamotani and Greber (1974) that the flowfield downstream of opposed jets was similar to that downstream of a single jet injected toward an opposite wall at half the distance between the jets. This is also confirmed by the experimental results in Srinivasan, Coleman, & White (1984). Thus for the symmetric case, $H_{eq} = (H_0)/2$.

In general, these flows can be modeled by calculating an effective duct height as proposed by Wittig, Elbahar, & Noll (1984), namely;

$$[H_{eq}]_{top} = (H_0)\left([(A_j/A_m)(J^{0.5})]_{top}\right)\Big/\left([(A_j/A_m)(J^{0.5})]_{top} + [(A_j/A_m)(J^{0.5})]_{bottom}\right)$$

and

$$[H_{eq}]_{bottom} = H_0 - [H_{eq}]_{top}$$

Effects Due to Curvature

The flow in a curved duct develops a free vortex, wherein $U = (const)/r$, with higher velocities near the inner wall than near the outer wall. The local momentum-flux ratio is thus

$$J_{local} = (4)(J)(r/(r_i + r_o))^2$$

where J is the momentum-flux ratio based on the uniform mainstream velocity.

The effective momentum-flux ratio for OD jets is defined to be the integrated average of the values of J_{local} over the outer half of the duct, and similarly the effective momentum-flux ratio for ID jets is defined to be the integrated average of the J_{local} values over the inner half of the duct. These values are:

$$J_{OD} = (J)\left(1 + (2)(C_{OD}) + (4)(C_{OD})^2\right)/3$$

$$J_{ID} = (J)\left(1 + (2)(C_{ID}) + (4)(C_{ID})^2\right)/3$$

where

$$C_{OD} = (1 + H_0/R_{ci})/(2 + H_0/R_{ci})$$

and

$$C_{ID} = 1/(2 + H_0/R_{CI})$$

Flow Area Convergence

This case is modeled by assuming that the accelerating mainstream will act to decrease the effective momentum-flux ratio as the flow proceeds downstream, thus:

$$J(x) = (J)[H(x)/H_0]^2$$

Note that the trajectory and the jet half-widths are calculated in terms of the duct height at the injection location, so must be scaled by the inverse of the convergence rate, $H_0/H(x)$, to give profiles in terms of the local duct height.

Orifice Aspect Ratio

It was observed by Srinivasan, Meyers, Coleman, & White (1985) that bluff slots resulted in slightly less jet penetration and more two-dimensional profiles than circular holes, and that streamlined slots resulted in slightly greater jet penetration and more three-dimensional profiles. This effect is modeled by using the ratio of the orifice spacing to the orifice width, S/W, in lieu of S/D in the correlation equations. For rectangular orifices with circular ends;

$$S/W = (S/D)[1 + (4/\pi)(AR - 1)]^{0.5} \quad \text{if} \quad AR > 1$$

and

$$S/W = (S/D)[1 + (4/\pi)(1/AR - 1)]^{0.5}/AR \quad \text{if} \quad AR < 1$$

where

$$AR = W/L$$

Slanted Slots

Two effects were noted in the experimental results for slanted slots, namely that the centerplanes shifted laterally with increasing downstream distance, and the axes of the kidney-shaped temperature contours were inclined with respect to the injection direction. The former is modeled as a function of momentum-flux ratio and downstream distance as:

$$dz/S = \sin[(\pi/2)(a)]$$

where

$$a = \min\left[1, (x/H_{eq})(J/26.4)^{0.25}\right]$$

The rotation effect observed in the experimental data is not modeled.

References

Atkinson, K.N., Khan, Z.A., and Whitelaw, J.H., 1982, "Experimental Investigation of Opposed Jets Discharging Normally into a Cross-stream," *Journal of Fluid Mechanics*, Vol. 115, pp. 493-504.

Bruce, T.W., Mongia, H.C., and Reynolds, R.S., 1979, "Combustor Design Criteria Validation," AiResearch Manufacturing Co., Phoenix, AZ, AiResearch 75-211682(38)-1, - 2, -3; (USARTL-TR-78-55A, B, and C).

Carrotte, J.F., and Stevens, S.J., 1990, "The Influence of Dilution Hole Geometry on Jet Mixing," *Journal of Engineering for Gas Turbines and Power*, Vol. 112, No. 1, pp. 73-75 (Also, ASME Paper 89-GT-292).

Claus, R.W., 1983, "Analytical Calculation of a Single Jet in Crossflow and Comparison with Experiment," AIAA Paper 83-0238, (Also, NASA TM-83027).

Claus, R.W. and Vanka, S.P., 1990, "Multigrid Calculations of a Jet in Crossflow," AIAA Paper 90-0444.

Cox, G.B. Jr., 1975, "An Analytical Model for Predicting Exit Temperature Profile from Ga Turbine Engine Annular Combustors," AIAA Paper 75-1307.

Cox, G.B. Jr., 1976, "Multiple Jet Correlations for Gas Turbine Engine Combustor Design," *Journal of Engineering for Power*, Vol. 98, No. 2, pp. 265-273.

Dwenger, R.D., 1990, "Laser Doppler Velocimeter Measurements and Laser Sheet Imaging in an Annular Combustor Model," M.S. Thesis, Purdue University.

Ferrell, G.B., Abujella, M.T., Busnaina, A.A., and Lilley, D.G., 1984, "Lateral Jet Injection into Typical Combustor Flowfields. AIAA Paper 84-0374.

Ferrell, G.B., Aoki, K., and Lilley, D.G., 1985, "Flow Visualization of Lateral Jet Injection into Swirling Crossflow," AIAA Paper 85-0059.

Ferrell, G.B. and Lilley, D.G., 1985, "Deflected Jet Experiments in a Turbulent Combustor Flowfield," Ph.D. Thesis, Oklahoma State University, NASA CR-174863.

Ferrell, G.B. and Lilley, D.G., 1985, "Turbulence Measurements of Lateral Jet Injection into Confined Tubular Crossflow," AIAA Paper 85-1102.

Holdeman, J.D., Walker, R.E., and Kors, D.L., 1973, "Mixing of Multiple Dilution Jets with a Hot Primary Airstream for Gas Turbine Combustors," AIAA Paper 73-1249, (Also, NASA TM X-71426).

Holdeman, J.D. and Walker, R.E., 1977, "Mixing of a Row of Jets with a Confined Crossflow," *AIAA Journal*, Vol. 15, No. 2, pp. 243-249 (see also, NASA TM-71821).

Holdeman, J.D., 1983, "Perspectives on the Mixing of a Row of Jets with a Confined Crossflow," AIAA Paper 83-1200, (Also, NASA TM-83457).

Holdeman, J.D., and Srinivasan, R., 1984, "Modeling of Dilution Jet Flowfields," Combustion Fundamentals Research, NASA CP-2309, pp. 175-187.

Holdeman, J.D., Srinivasan, R., and Berenfeld, A., 1984, "Experiments in Dilution Jet Mixing," *AIAA Journal*, Vol. 22, No. 10, pp. 1436-1443 (Also, NASA TM-83434).

Holdeman, J.D., Srinivasan, R., Coleman, E.B., Meyers, G.D., and White, C.D., 1985, "Experiments in Dilution Jet Mixing—Effects of Multiple Rows and Non-circular Orifices," AIAA Paper 85-1104.

Holdeman, J.D., 1986, "Experiments and Modeling of Dilution Jet Flowfields," NASA-Chinese Aeronautical Establishment (CAE) Symposium, NASA CP-2433, pp. 149-174.

Holdeman, J.D., and Srinivasan, R., 1986, "Modeling Dilution Jet Flowfields," *Journal of Propulsion and Power*, Vol. 2, No. 1, pp. 4-10 (see also, AIAA Paper 84-1379, NASA TM-83708).

Holdeman, J.D., and Srinivasan, R., 1986, "Perspectives on Dilution Jet Mixing," AIAA Paper 86-1611, (Also, NASA TM-87294).

Holdeman, J.D., Srinivasan, R., Coleman, E.B., Meyers, G.D., and White, C.D., 1987, "Effects of Multiple Rows and Noncircular Orifices on Dilution Jet Mixing," *Journal of Propulsion and Power*, Vol. 3, No. 3, pp. 219-226 (see also, AIAA Paper 85-1104, NASA TM-86996).

Holdeman, J.D., Reynolds, R., and White, C., 1987, "A Numerical Study of the Effects of Curvature and Convergence on Dilution Jet Mixing," AIAA Paper 87-1953, (Also, NASA TM-89878).

Holdeman, J.D., Mongia, H.C., and Mularz, E.J., 1988, "Assessment, Development, and Application of Combustor Aerothermal Models," NASA TM-100290.

Holdeman, J.D., Srinivasan, R., and White, C.D., 1988, "An Empirical Model of the Effects of Curvature and Convergence on Dilution Jet Mixing," AIAA Paper 88-3180, (Also, NASA TM-100896).

Holdeman, J.D., Srinivasan, R., Reynolds, R., and White, C.D., 1991, "Studies of the Effects of Curvature on Dilution Jet Mixing," *Journal of Propulsion and Power*, Vol. 7, No. 4, (see also, AIAA-87-1953, NASA TM-89878; AIAA-88-3180, NASA TM-100896).

Kamotani, Y. and Greber, I, 1973, "Experiments on Confined Turbulent Jets in Cross Flow," AIAA Paper 73-647.

Kamotani, Y. and Greber, I, 1974, "Experiments on Confined Turbulent Jets in Cross Flow," NASA CR-2392.

Karagozian, A.K., 1986, "An Analytical Model for the Vorticity Associated with a Transverse Jet," *AIAA Journal*, Vol. 24, No. 3, pp. 429-436.

Kenworthy, M.J., Correa, S.M., and Burrus, D.L., 1983, "Aerothermal Modeling Phase I—Final Report," Vols. 1-2, NASA CR-168296.

Khan, Z.A., McGuirk, J.J., and Whitelaw, J.H., 1982, "A Row of Jets in a Crossflow," Fluid Dynamics of Jets with Application to V/STOL, AGARD-CP-308, pp. 10-1 to 10-11.

Launder, B.E., Reece, G.J., and Rodi, W., 1975, "Progress in the Development of a Reynolds-Stress Turbulence Closure," *Journal of Fluid Mech.*, Vol. 68, No. 3, pp. 537-566.

Lilley, D.G., 1986, "Lateral Jet Injection Into Typical Combustor Flowfields," NASA CR-3997.

Lipshitz, A. and Greber, I., 1981, "Turbulent Jet Patterns in Accelerating Flows," AIAA Paper 81-0348.

Lipshitz, A. and Greber, I., 1984, "Dilution Jets in Accelerated Crossflows," NASA CR-174717.

McMurry, C.B. and Lilley, D.G., 1986, "Experiments on Opposed Lateral Jets Injected into Swirling Crossflow," M.S. Thesis, Oklahoma State University, NASA CR-175041.

McMurry, C.B., Ong, L.H., and Lilley, D.G., 1987, "Two Opposed Lateral Jets Injected Into Swirling Crossflow," AIAA Paper 87-0307.

Mongia, H.C., Reynolds, R.S., and Srinivasan, R., 1986, "Multidimensional Gas Turbine Combustion Modeling: Applications and Limitations," *AIAA Journal*, Vol. 24, No. 6, pp. 890-904.

NASA, 1969, Analysis of a Jet in a Subsonic Crosswind. NASA SP-218.

Nikjooy, M., Karki, K.C., and Mongia, H.C., 1990, "Calculation of Turbulent Three-Dimensional Jet-Induced Flow in a Rectangular Enclosure," AIAA Paper 90-0684.

Novick, A.S., Arvin, J.R., and Quinn, R.E., 1980, "Development of a Gas Turbine Combustor Dilution Zone Design Analysis," *Journal of Aircraft*, Vol. 17, No. 10, pp. 712-718.

Novick, A.S., and Troth, D.L., 1981, "Low NO_x Heavy Fuels Combustor Concept Program," DDA-EDR-10594, Detroit Diesel Allison Division, General Motors Corp., NASA CR-165367, DOE-NASA-0148-1.

Ong, L.H., and Lilley, D.G., 1986, "Measurements of a Single Lateral Jet Injected into Swirling Crossflow," M.S. Thesis, Oklahoma State University, NASA CR-175040.

Ong, L.H., McMurry, C.B., and Lilley, D.G., 1986, "Hot-Wire Measurements of a Single Lateral Jet Injected into Swirling Crossflow," AIAA Paper 86-0055.

Patankar, S.V., 1980, *Numerical Heat Transfer and Fluid Flow*, McGraw-Hill/Hemisphere.

Reynolds, R. and White, C., 1987, "Transition Mixing Study, Final Report," Garrett-21-5723, The Garrett Turbine Engine Co., Phoenix, AZ, NASA CR-175062.

Richards, C.D. and Samuelsen, G.S., 1990, "The Interaction of Primary Jets with a Swirl-Induced Recirculation Zone," AIAA Paper 90-0455.

Richards, C.D. and Samuelsen, G.S., 1990, "The Role of Primary Jets in the Dome Region Aerodynamics of a Model Can Combustor," ASME Paper 90-GT-142.

Richards, C.D. and Samuelsen, G.S., 1990, "The Role of Primary Jet Injection on Mixing in Gas Turbine Combustion," *23rd Symposium (International) on Combustion*, The Combustion Institute, to be published.

Richards, C.D., 1990, "An Investigation of Radial Jets Injected Into a Cylindrical Duct Flow," Ph.D. Thesis, University of California-Irvine, Irvine, CA.

Riddlebaugh, S.M., Lipshitz, A., and Greber, I., 1982, "Dilution Jet Behavior in the Turn Section of a Reverse-Flow Combustor," AIAA Paper 82-0192, (Also, NASA TM-82776).

Smith, C.E., 1990, "Mixing Characteristics of Dilution Jets in Small Gas Turbine Combustors," AIAA Paper 90-2728.

Smith, C.E., Talpallikar, M.V., and Holdeman, J.D., 1991, "Jet Mixing in Reduced Flow Areas for Lower Emissions in Gas Turbine Combustors," AIAA Paper 91-2460, Sacramento, CA.

Spalding, D.B., 1972, "A Novel Finite-Difference Formulation for Differential Expressions Involving both First and Second Derivatives," *International Journal for Numerical Methods in Engineering*, Vol. 4, pp. 551-559.

Srinivasan, R., Reynolds, R., Ball, I., Berry, R., Johnson, K., and Mongia, H.C., 1983, "Aerothermal Modeling Program: Phase I, Final Report," Garrett Turbine Engine Co., Phoenix, AZ, Garrett-21-4742, -1, -2; NASA CR-168243-VOL-1, -2.

Srinivasan, R., Berenfeld, A., and Mongia, H.C., 1982, "Dilution Jet Mixing Program, Phase I Report," Garrett-21-4302, The Garrett Turbine Engine Co., Phoenix, AZ, NASA CR-168031.

Srinivasan, R., Coleman, E., and Johnson, K., 1984, "Dilution Jet Mixing Program, Phase II Report," Garrett-21-4804, The Garrett Turbine Engine Co., Phoenix, AZ, NASA CR-174624.

Srinivasan, R., Meyers, G., Coleman, E., and White, C., 1985, "Dilution Jet Mixing, Phase III Report," Garrett-21-5418, Garrett Turbine Engine Co., Phoenix, AZ, NASA CR-174884.

Srinivasan, R. and White, C., 1986, "Dilution Jet Mixing, Supplementary Report," Garrett-21-5705, Garrett Turbine Engine Co., Phoenix, AZ, NASA CR-175043.

Srinivasan, R. and White, C., 1988, "Transition Mixing Study Empirical Model Report," Garrett-21-6689, Garrett Engine Co., Phoenix, AZ, NASA CR-182139.

Stevens, S.J. and Carrotte, J.F., 1990, "Experimental Studies of Combustor Aerodynamics, Part I: Mean Flowfields," *Journal of Propulsion and Power*, Vol. 6, No. 3, pp. 297-304 (see also, AIAA Paper 87-1827, "The Influence of Dilution Hole Aerodynamics on the Temperature Distribution in a Combustor Dilution Zone," June 1987).

Stevens, S.J. and Carrotte, J.F., 1990, "Experimental Studies of Combustor Dilution Zone Aerodynamics, Part II: Jet Development," *Journal of Propulsion and Power*, Vol. 6, No. 4, pp. 503-511, (see also, AIAA Paper 88-3274, July 1988).

Sturgess, G.J., 1983, "Aerothermal Modeling Phase I Final Report," Pratt & Whitney Aircraft, East Hartford, CT, PWA-5907-19, NASA CR-168202.

Sullivan, J.P., Barron, D., Seal, M., Morgan, D., and Murthy, S.N.B., 1989, "Primary Zone Dynamics in a Gas Turbine Combustor," AIAA Paper 89-0489.

Talpallikar, M.V., Smith, C.E., and Lai, M.C., 1990, "Rapid Mix Concepts for Low Emission Combustors in Gas Turbine Engines," NASA CR-185292, CFD Research Corp., Huntsville, AL.

Talpallikar, M.V., Smith, C.E., Lai, M.C., and Holdeman, J.D., 1991, "CFD Analysis of Jet Mixing in Low NO_x Flametube Combustors," ASME Paper 91-GT-217.

Vranos, A., and Liscinsky, D.S., 1988, "Planar Imaging of Jet Mixing in Crossflow," AIAA Journal, Vol. 26, No. 11, pp. 1297-1298.

Vranos, A., Liscinsky, D., True, B., and Holdeman, J.D., 1991, "Experimental Study of Cross-Stream Mixing in a Cylindrical Duct," AIAA Paper 91-2459.

Vranos, A., and Liscinsky, D.S., 1991, "Enhanced Mixing Study: Experiments in a Cylindrical Duct," United Technologies Research Center, East Hartford, CT, NASA CR-187141.

Walker, R.E. and Kors, D.L., 1973, "Multiple Jet Study," Aerojet Liquid Rocket Co., Sacramento, CA, NASA CR-121217.

Walker, R.E., Kors, D.L., and Holdeman, J.D., 1973, "Mixing of Multiple Jets of Cooling Air With Simulated Combustion Gases," 10th JANNAF Combustion Meeting, Vol. 2, CPIA-PUBL-243-VOL-II, Chemical Propulsion Information Agency, Laurel, MD, pp. 377-396.

Walker, R.E. and Eberhardt, R.G., 1975, "Multiple Jet Study Data Correlations," Aerojet Liquid Rocket Co., Sacramento, CA, NASA CR-134795.

Wittig, S.L.K., Elbahar, O.M.F., and Noll, B.E., 1984, "Temperature Profile Development in Turbulent Mixing of Coolant Jets with a Confined Hot Cross-Flow," *Journal of Engineering for Gas Turbines and Power*, Vol. 106, No. 1, pp. 193-197 (see also, ASME Paper No. 83-GT-39).

Zizelman, J., 1985, "Dilution Jet Configurations in a Reverse Flow Combustor," M.S. Thesis, Case Western Reserve Univ., Cleveland, OH, NASA CR-174888.

TABLE 1.—RANGES OF FLOW AND GEOMETRIC VARIABLES ON WHICH MODEL IS BASED

Independent variables:	Range
Downstream distance, x/H_0	0 to 2
Density ratio, DR	0.5 to 2.2
Momentum-flux ratio, J	5 to 105
Orifice diameter, H_0/D	4 to 16
Orifice transverse (circumferential) spacing (S/D)	2 to 6
Orifice row axial offset, S_y/H_0	0.25 to 0.5
Orifice aspect ratio	0.36 to 2.8
Area ratio (exit/inlet)	0.33 to 1
Radius of curvature in x-r plane, R_{cl}/H_0	0.25 to ∞
Radius of curvature in r-z plane, R_y/H_0	0 to ∞
Variable mainstream, θ	0 to 0.5
Derived variables:	
Orifice spacing, S/H_0	0.125 to 1
A_j/A_m	0.025 to 0.1
w_j/w_T	0.075 to 0.36
$C = (S/H_0)\sqrt{(J)}$	0.5 to 10

TABLE 2.—FLOW AND GEOMETRIC CONDITIONS FOR STRAIGHT DUCT EXPERIMENTS

Figure	Case[a]	Description	Plate[b]	S/D	H_0/D	S/H_0	A_j/A_m	C_d	DR	J	w_j/w_m	w_j/w_T	C[c]
2, 12(a), 21(a)	III-22		C	2	4	0.5	0.098	0.76	2.2	26.2	0.57	0.36	2.56
6(a), 7(a)	I-5		L	2	8	.25	.049	.6	2.1	22.4	.20	.17	1.18
6(b), 7(b), 11(b)	I-4		H	4	4	1	.049	.67	2.2	23.5	.24	.19	4.85
8(a)	I-3		H	4	4	1	.049	.73	2.1	5.3	.12	.11	2.30
8(b), 17(b), 24(a)	I-7		A	4	8	0.5	.025	.61	2.2	28.4	.12	.11	2.66
8(c), 16(b)	I-6		L	2	8	.25	.049	.61	2.3	92.7	.44	.30	2.41
9(a)	II-50		B	2.8	5.7	.5	.049	.71	2.2	25.4	.26	.20	2.52
9(b), 10(a), 19(a), 26(a)	I-2		C	2	4	.5	.098	.61	2.1	18.6	.37	.27	2.16
10(b)	II-26	symmetric convergence	C	2	4	.5	.098	.60	2.0	26.4	.43	.30	2.56
10(c)	II-34	injection wall convergence	C	2	4	.5	.098	.61	2.2	26.4	.46	.31	2.57
11(a)	II-32	square holes	I	4	4	1	.049	.67	2.1	24.2	.23	.19	4.92
12(a)	III-2	streamlined slots	D	2	4	0.5	.098	.71	2.2	26.5	.53	.35	2.57
12(b)	III-3	bluff slots	E	2	4	0.5	.098	.9	2.2	26.6	.68	.40	2.58
12(c), 13(b), 14	III-19	slanted slots	F	2	4	0.5	.098	.66	2.2	27.1	.50	.33	2.60
15(a)	II-45(a)	wide slot	K	—	9.9	—	.10	.75	2.2	6.7	.28	.22	—
15(b), 18(b)	I-1		C	2	4	0.5	.098	.67	2.1	5.0	.21	.18	1.12
16(a)	II-31(c)	narrow slot	J	—	19.8	—	.05	.72	2.1	105.4	.39	.35	—
17(a)	I-12	hot jets	A	4	8	0.5	.025	.65	0.65	22.7	.06	.06	2.38
17(c)	I-8	ambient jets	A	4	8	↓	.025	.61	2.3	96.0	.22	.18	4.90
18(a)	I-9	hot jets	C	2	4	↓	.098	.61	0.62	22.7	.22	.18	2.38
19(b), 20	I-13	top cold	C	2	4	↓	.098	.61	1.8	31.8	.45	.31	2.82
19(c)	I-17	top hot	C	2	4	↓	.098	.68	1.8	24.4	.45	.31	2.47
21(b), 22	III-6	double/in-line	M	2.8	5.7	↓	.049	.65	2.2	26.3	.24	.33	2.56
				2.8	5.7	↓	.049	.66	2.2	26.9	.25	—	2.59
21(c), 23	III-11	double/dissimilar	N	2.8	5.7	0.5	.049	.69	2.2	26.8	.26	.34	2.58
				2	8	0.25	.049	.7	2.2	26.6	.26		1.29
21(d)	III-9	double/staggered	O	4	4	1	.049	.65	2.2	26.8	.24	.33	5.18
				4	4	1	.049	.68	2.2	26.7	.26		5.17
24(b), 25	II-2	opposed/in-line	L&L	2	8	0.25	.098	.65	2.1	25.0	.46	.32	1.25
26(b), 27	II-28	opposed/staggered	G&H	4	4	1	.098	.65	2.1	26.4	.48	.32	5.14

[a]Srinivasan & White (1986)

[b]See Fig. 3

[c]$C = (S/H0)\sqrt{(J)}$

TABLE 3.—FLOW AND GEOMETRY CONDITIONS FOR NUMERICAL STUDIES

Figure	Case[a]	J	S/H_0	H_0/D	R_{ci}/H_0	R_i/H_0	Area Ratio	Configuration
28(a),(d),(e)	38	6.6	0.5	4	Infinity	Infinity	1	Aligned/slanted
28(b),(f),(g)	39	6.6			Infinity			Crossed/slanted
28(c),(h),(i); 35(a),(c),(d); 36(a)	30	6.6			Infinity			Opposed/in-line
29(a),(e); 30(a),(e); 31(d),(g); 32(d),(g)	9	26.4			0.5			ID jets
29(b),(c),(f); 30(b),(c),(f)	12				Infinity			One-side
29(d),(h); 30(d),(h); 31(a),(d); 32(a),(d)	1				0.5			OD jets
31(b),(c),(f); 32(b),(c),(f)	18		1.0					Opposed/staggered
33(a),(c); 34(a)	37		0.25	8				Opposed/in-line
33(b),(d); 34(b)	10	6.6	0.5	4				
35(b),(e); 36(b)	29				0.25			
37(a),(b); 38(a)	21				Annulus	1		
39(a),(d),(e); 40(a),(d),(e)	31				Infinity	Infinity	1/3	
39(b),(f); 40(b),(f)	33				0.25	Infinity	1/3	
39(c),(g); 40(c),(g)	35				0.25	2.2	1/3	
41(a),(b),(c); 42(a),(b),(c)	41	26.4			Can	Infinity	1	OD jets

[a]Reynolds and White (1987), Srinivasan and White (1988).

TABLE 4.—SPACING AND MOMENTUM-FLUX RATIO RELATIONSHIPS

Configuration	$C = (S/H_0)\sqrt{(J)}$
Single-side injection:	
Under-penetration	<1.25
Optimum	2.5
Over-penetration	>5.0
Opposed rows of jets:	
In-line optimum	1.25
Staggered optimum	5.0

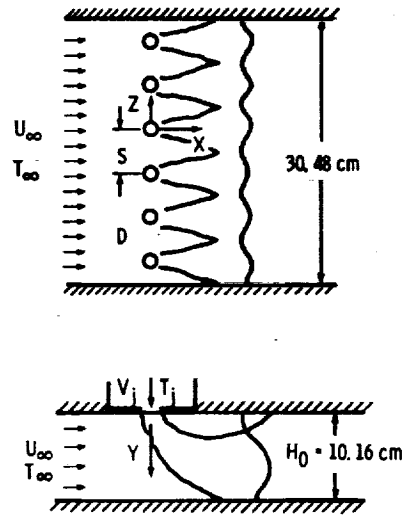

Figure 1. - Schematic of multiple jet flow.

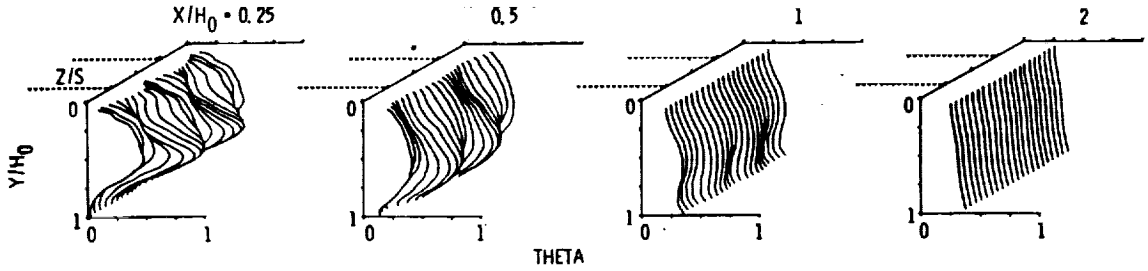

Figure 2. - Experimental mean temperature distributions (J = 26.2, S/H_0 = 0.5, H_0/D = 4).

	S/H_o	H_o/D	S_x/H_o	Type
A	0.5	8	—	
B	.5	5.7	—	
C	.5	4	—	
D	.5	4	—	0° Slot
E	.5	4	—	90° Slot
F	.5	4	—	45° slot
G	1.0	4	—	
H	1.0	4	—	
I	1.0	4	—	Square
J	—	9.9	—	2-D Slot
K	—	19.8	—	2-D slot
L	.25	8	—	
M	.5	5.7	0.5	In-Line
	.5	5.7	—	
N	.5	5.7	.25	Dissimilar
	.25	8	—	
O	1.0	4	.5	Staggered
	1.0	4	—	

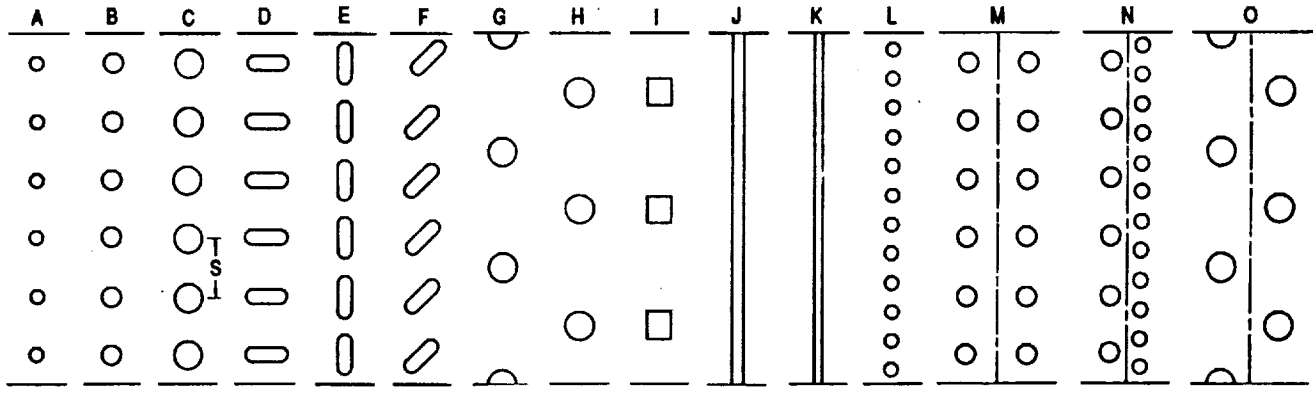

Figure 3.—Orifice configurations.

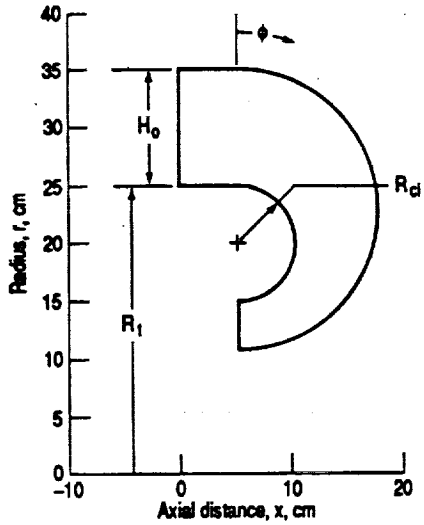

(a) Transition duct parameters.

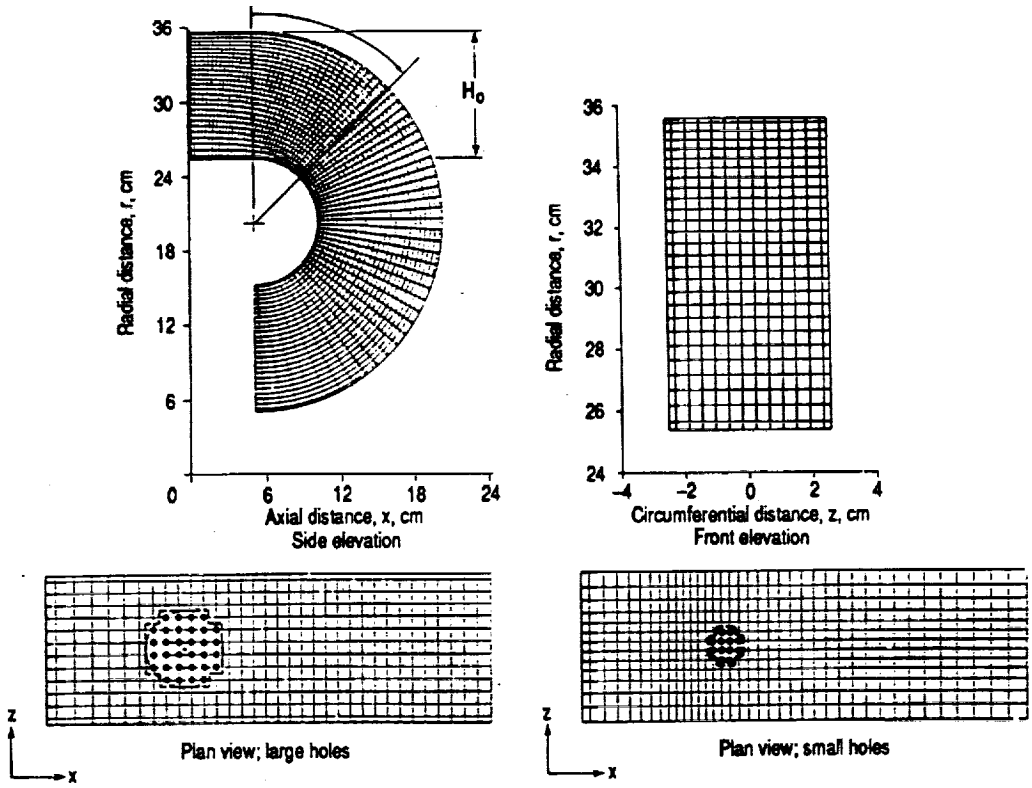

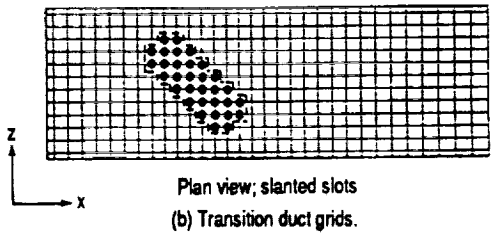

(b) Transition duct grids.

Figure 4.—Parameters for dilution jet mixing studies.

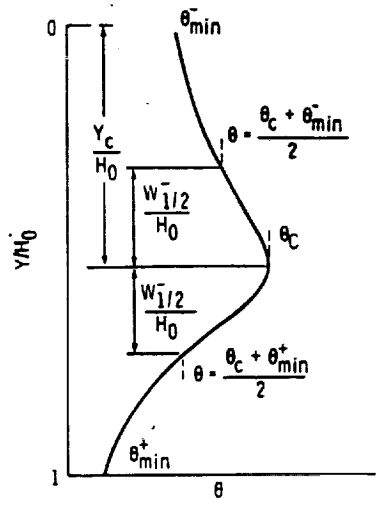

Figure 5. - Schematic of typical vertical temperature profile showing scaling parameters in empirical model.

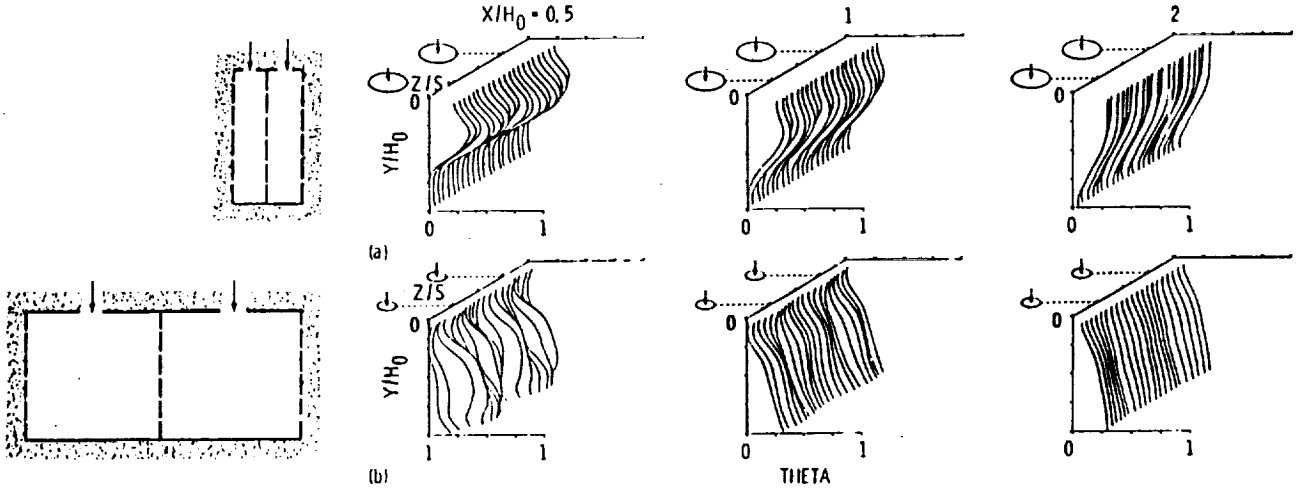

(a) $S/H_0 = 0.25$, $H_0/D = 8$, $J = 22.4$.
(b) $S/H_0 = 1$, $H_0/D = 4$, $J = 23.5$.

Figure 6 - Effect of varying orifice spacing at constant area on temperature distributions ($A_j/A_m = 0.05$).

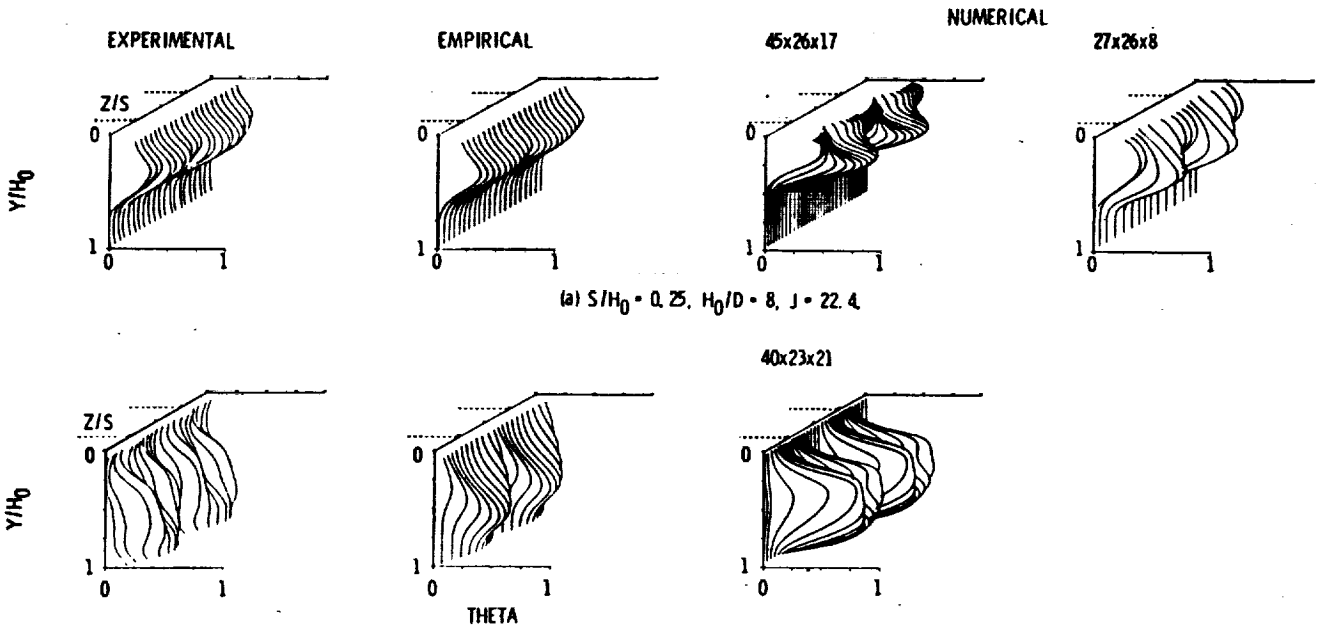

Figure 7. - Effect of varying orifice spacing at constant area on temperature distributions at $X/H_0 = 0.5$ ($A_j/A_m = 0.05$).

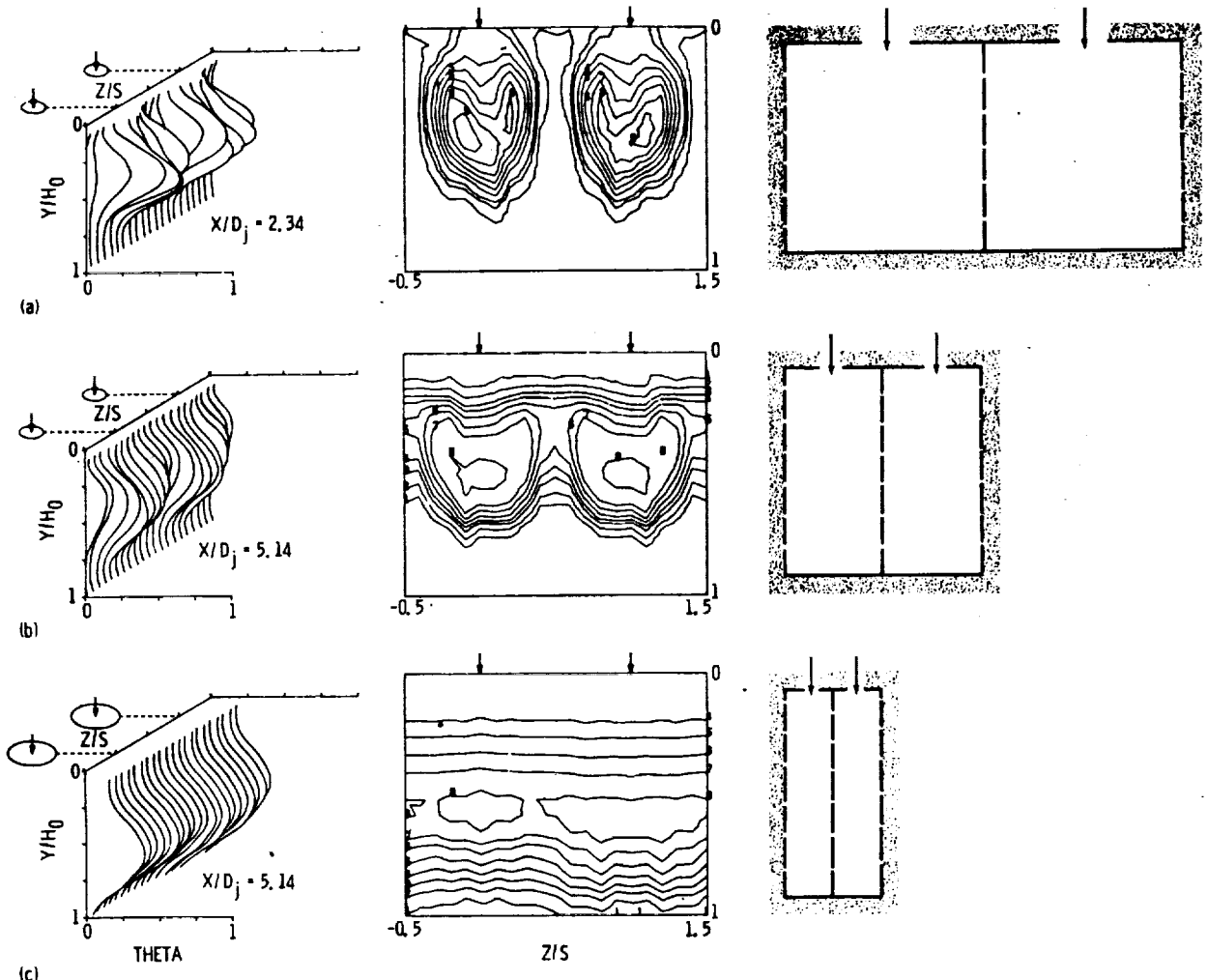

(a) $S/H_0 = 1$, $H_0/D = 4$, $A_j/A_m = 0.05$, $J = 5.3$.
(b) $S/H_0 = 0.5$, $H_0/D = 8$, $A_j/A_m = 0.025$, $J = 28.4$.
(c) $S/H_0 = 0.25$, $H_0/D = 8$, $A_j/A_m = 0.05$, $J = 92.7$.

Figure 8.—Oblique profile plots and isotherm contours at $X/H_0 = 0.5$ for coupled orifice spacing and momentum–flux ratio.

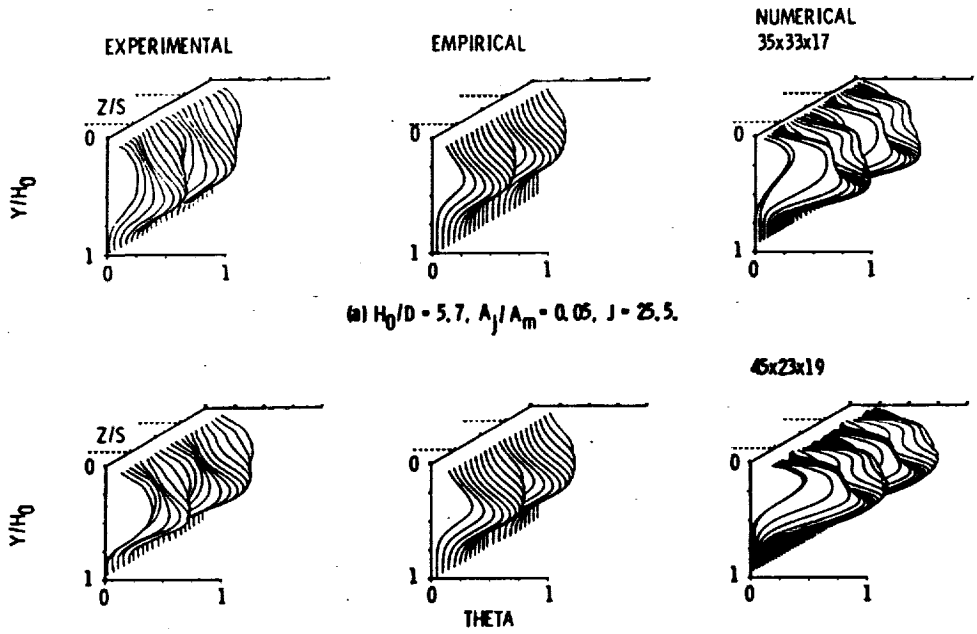

Figure 9. - Effect of varying orifice diameter at constant spacing on temperature distributions at $X/H_0 = 0.5$ ($S/H_0 = 0.5$).

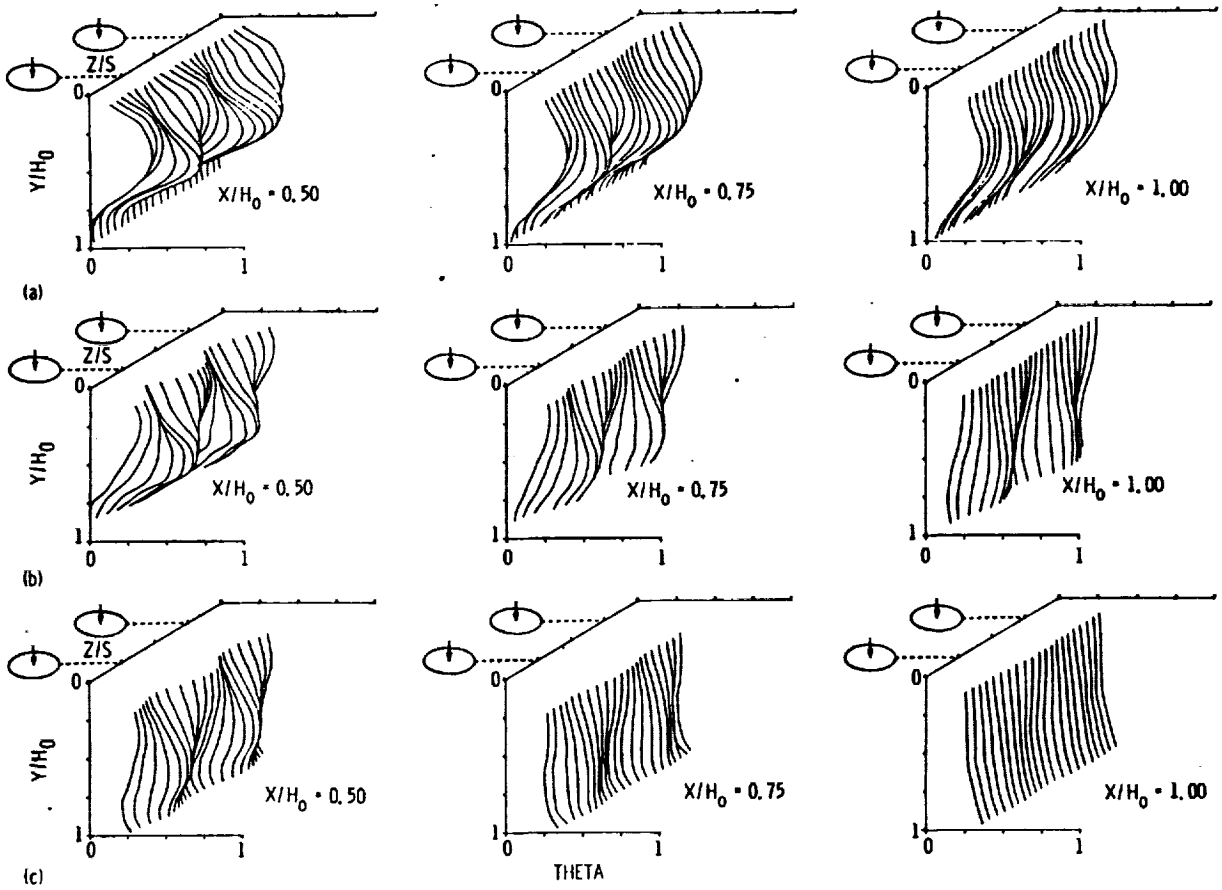

(a) Straight duct; J = 18.6.
(b) Symmetric convergence (0.5cm/cm); J = 26.4.
(c) Injection wall convergence (0.5cm/cm); J = 26.4.

Figure 10. - Influence of flow area convergence on temperature profiles ($S/H_0 = 0.5$, $H_0/D = 4$, $A_j/A_m = 0.098$).

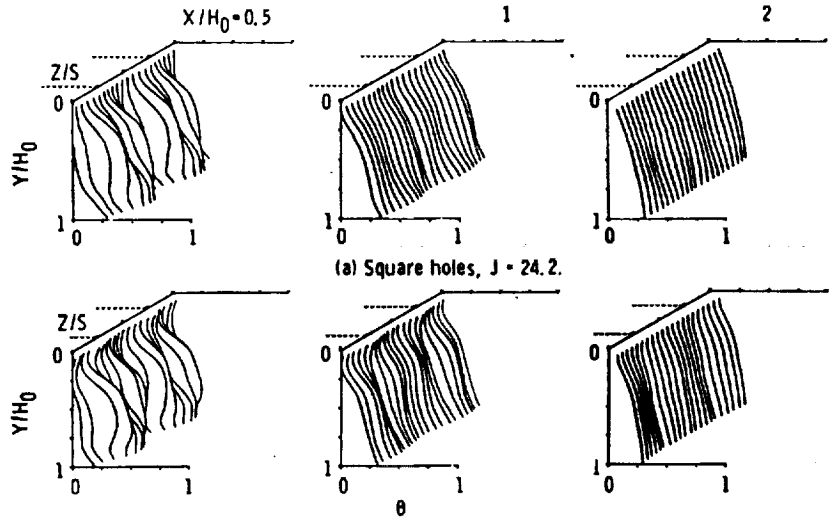

(a) Square holes, J = 24.2.

(b) Round holes, J = 23.5.

Figure 11. - Comparison of temperature distributions downstream of square and round holes: $S/H_0 = 1$, $H_0/D = 4$.

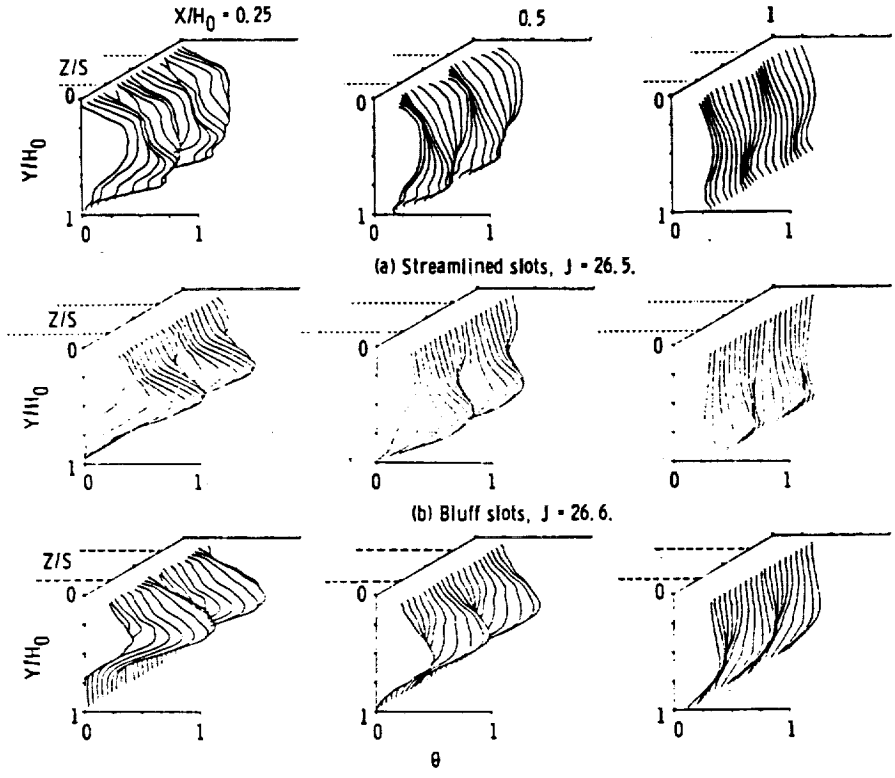

(a) Streamlined slots, J = 26.5.

(b) Bluff slots, J = 26.6.

(c) 45-deg slots, J = 27.1.

Figure 12. - Comparison of 3-D oblique temperature distributions for equivalent-area streamlined, bluff, and slanted slots at intermediate momentum flux-ratios: $S/H_0 = 0.5$, $H_0/D = 4$.

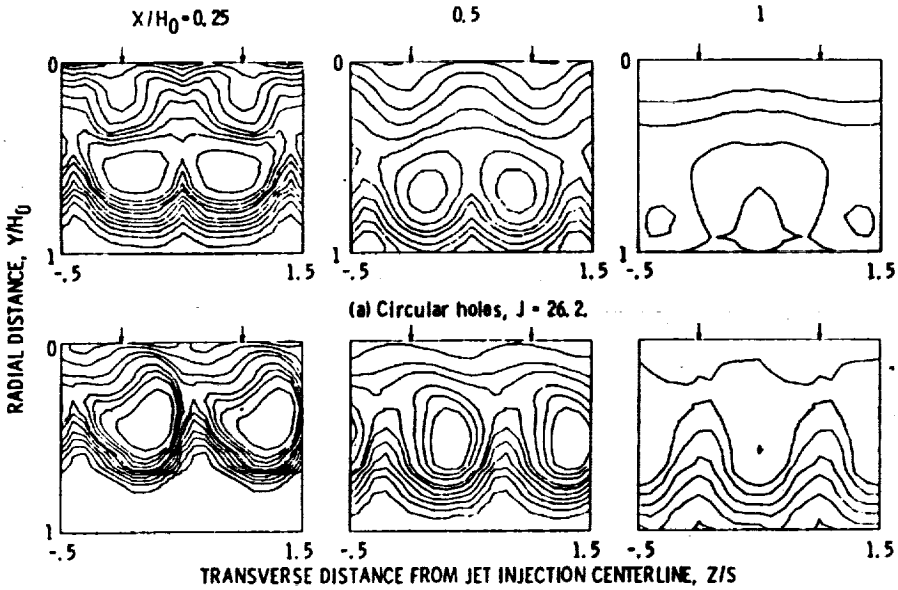

Figure 13. - Comparisons of isotherm contours for circular holes and 45-deg slanted slots at intermediate momentum flux ratios; $S/H_0 = 0.5$, $H_0/D = 4$.

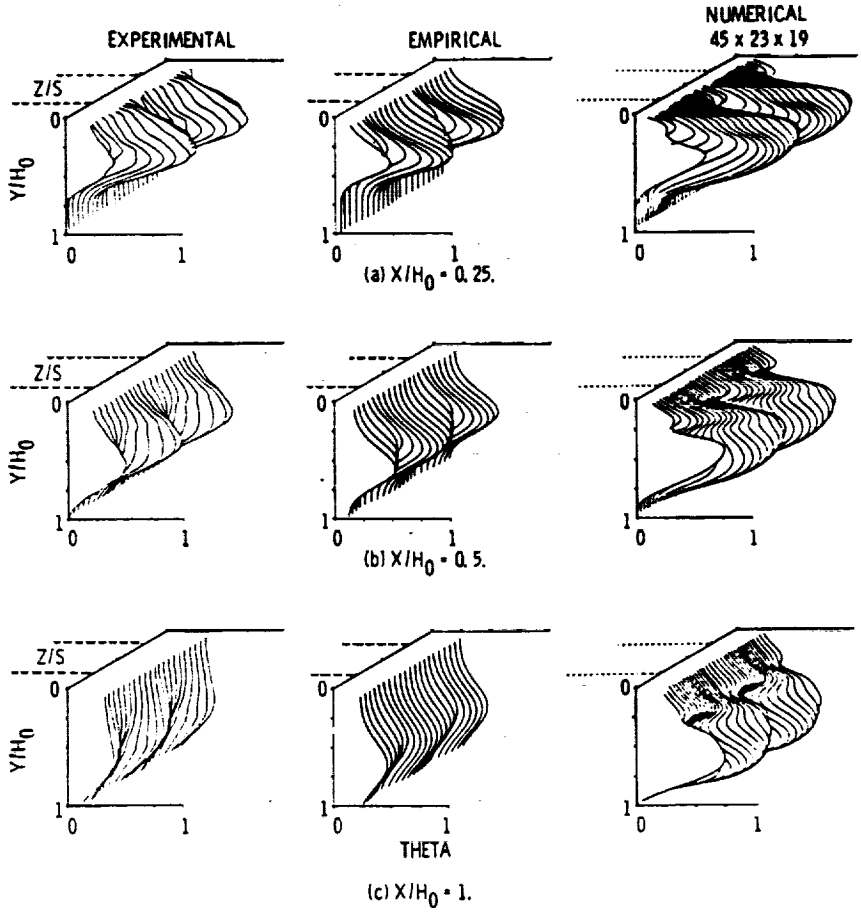

Figure 14. - Temperature distributions for slanted slots at an intermediate momentum flux ratio ($S/H_0 = 0.5$, $H_0/D = 4$, $J = 27.1$).

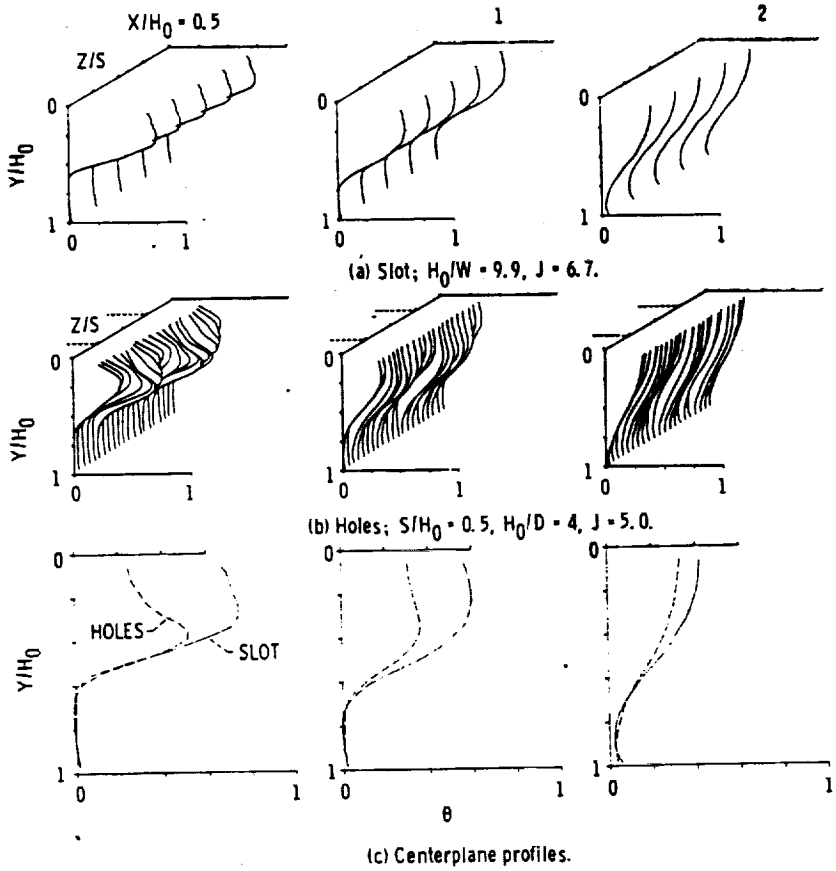

Figure 15. - Comparison of temperature distributions for a wide 2-D slot and closely-spaced holes at low momentum flux ratios.

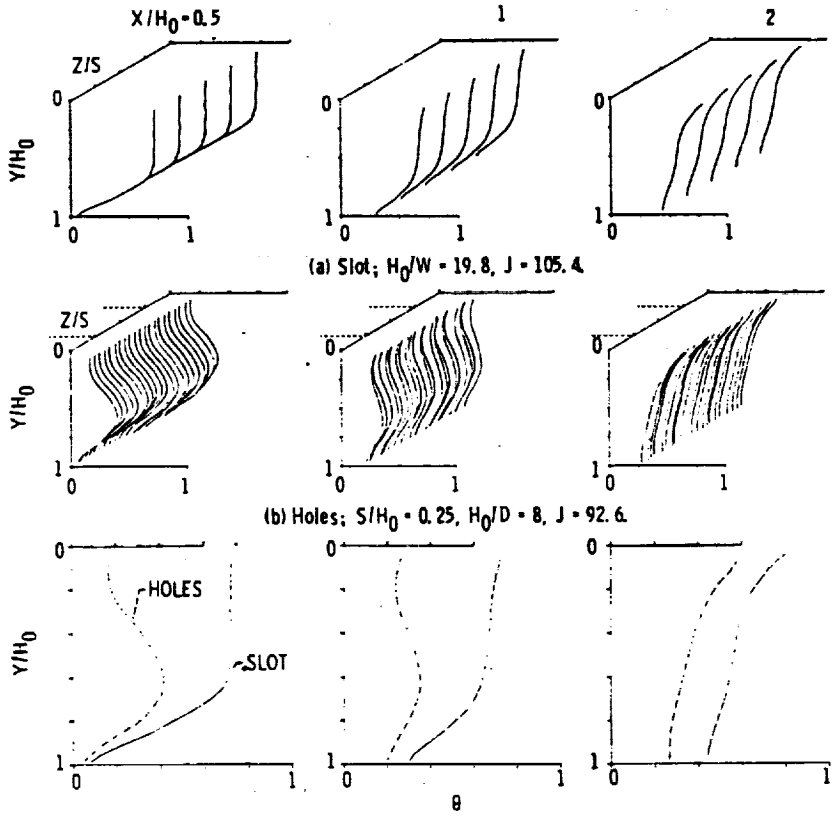

(c) Centerplane profiles.

Figure 16. - Comparison of temperature distributions for a narrow 2-D slot and closely-spaced holes at high momentum flux ratios.

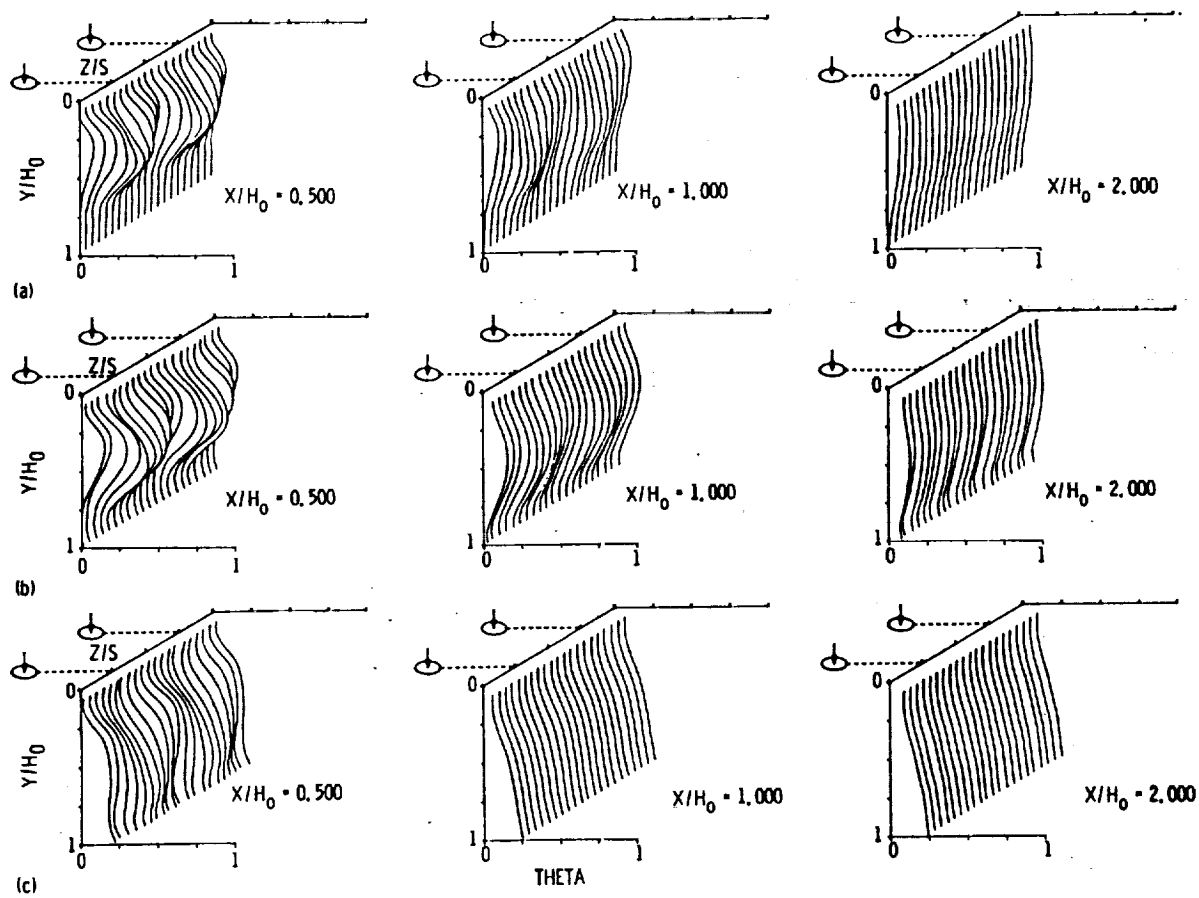

(a) Hot-jets/ambient-mainstream; DR = 0.65, J = 22.7, R = 5.5, w_j/w_T = 0.062.
(b) Ambient-jets/hot-mainstream; DR = 2.2, J = 28.4, R = 3.6, w_j/w_T = 0.105.
(c) Ambient-jets/hot-mainstream; DR = 2.3, J = 96.0, R = 6.5, w_j/w_T = 0.181.

Figure 17.—Effects of density,momemtum-flux, and velocity ratios on temperature profiles: S/H_0 = 0.5, H_0/D = 8, A_j/A_m = 0.025.

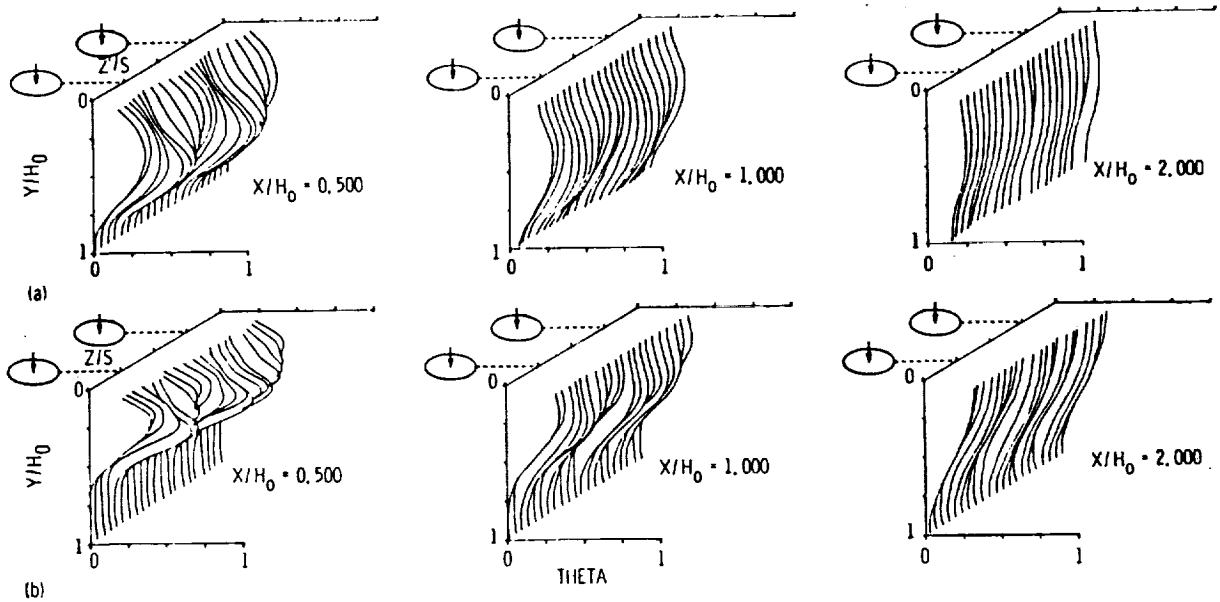

(a) Hot-jets/ambient-mainstream; DR = 0.62, J = 22.7, M = 3.8, w_j/w_T = 0.183.
(b) Ambient-jets/hot-mainstream; DR = 2.2, J = 5.0, M = 3.2, w_j/w_T = 0.176.

Figure 18.—Effects of density and mass-flux ratios on temperature profiles: S/H_0 = 0.5, H_0/D = 8, A_j/A_m = 0.25

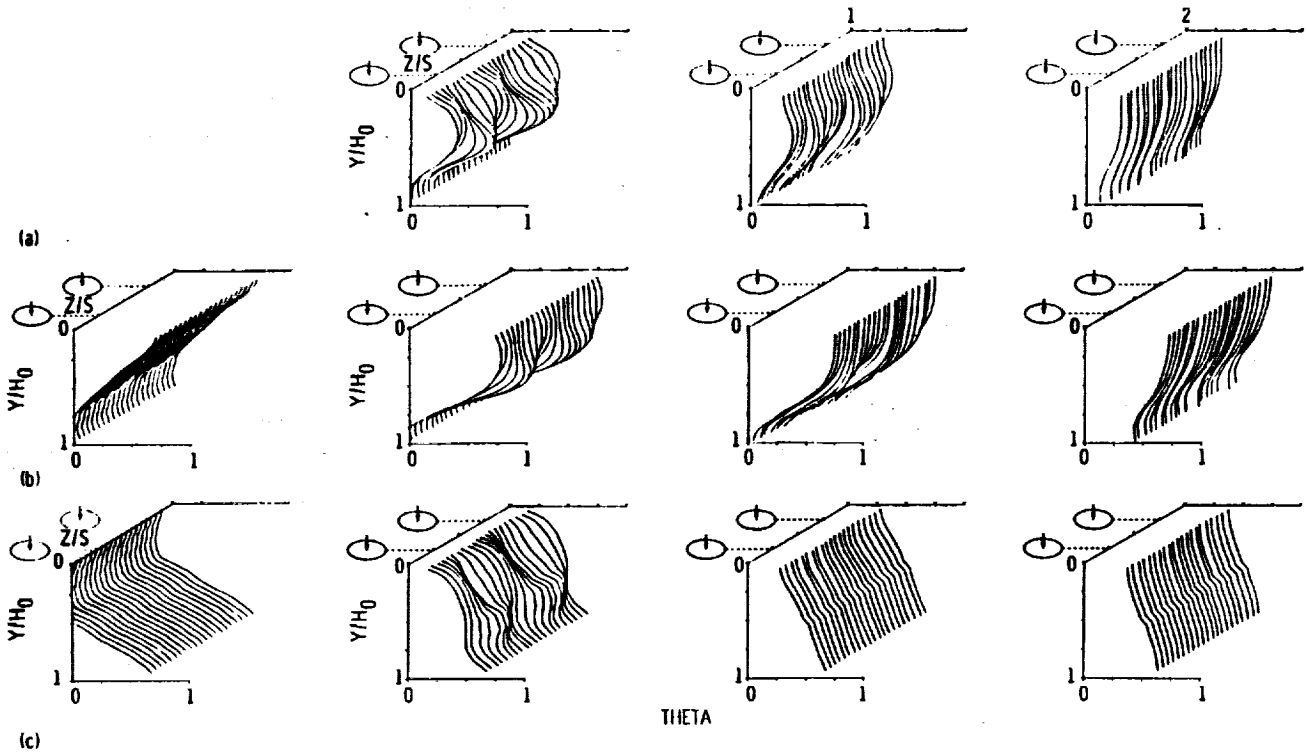

(a) Isothermal mainstream; J = 18.6.
(b) Top cold; J = 31.3.
(c) Top hot; J = 24.4.

Figure 19. - Influence of non-isothermal mainstream on temperature profiles ($S/H_0 = 0.5$, $H_0/D = 4$, $A_j/A_m = 0.098$).

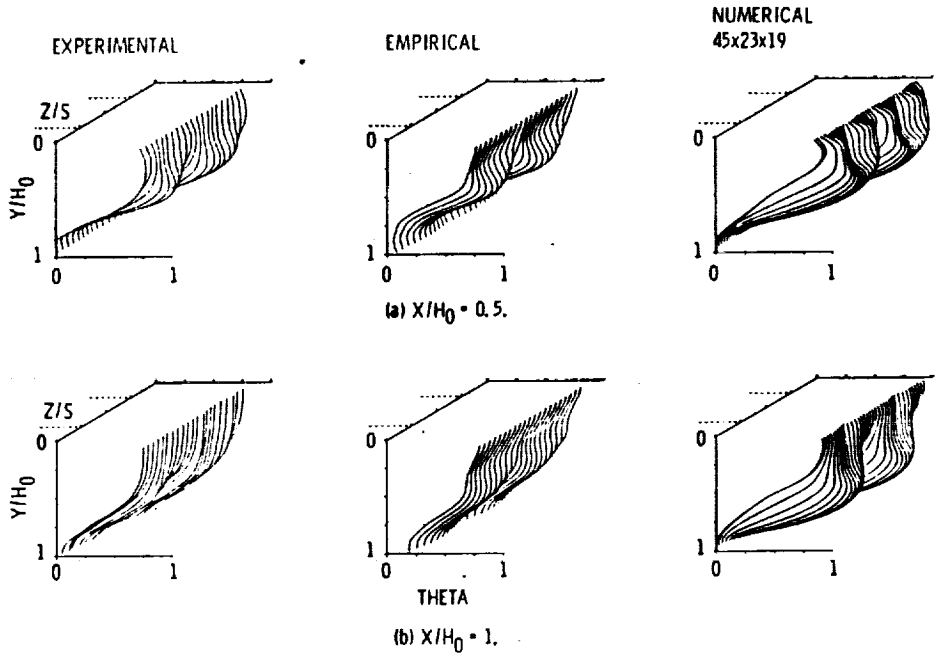

(a) $X/H_0 = 0.5$.

(b) $X/H_0 = 1$.

Figure 20. - Temperature distribution for jets injected into a non-isothermal mainstream; top cold ($S/H_0 = 0.5$, $H_0/D = 4$, $J = 31.3$).

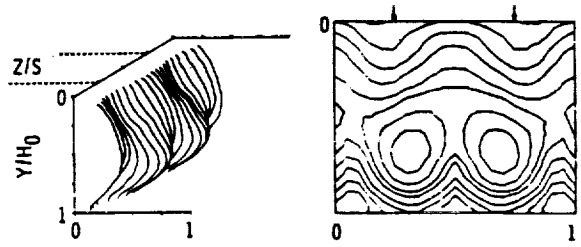

(a) Single row; $S/H_0 = 0.5$, $H_0/D = 4$, $J = 26.2$

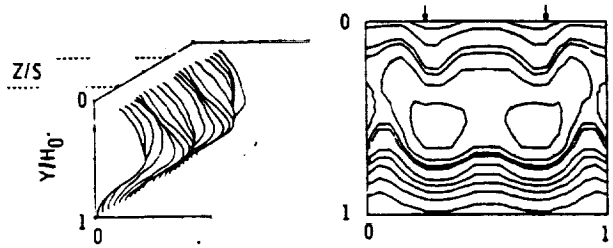

(b) Double row of in-line holes; $S_x/H_0 = 0.5$; Row 1: $S/H_0 = 0.5$, $H_0/D = 5.7$, $J = 26.3$. Row 2: $S/H_0 = 0.5$, $H_0/D = 5.7$, $J = 26.9$.

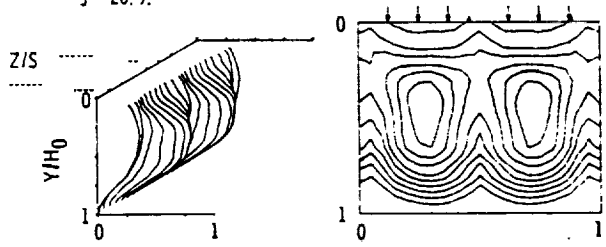

(c) Double row of disimilar holes; $S_x/H_0 = 0.25$; Row 1: $S/H_0 = 0.5$, $H_0/D = 5.7$, $J = 26.8$. Row 2: $S/H_0 = 0.25$, $H_0/D = 8$, $J = 26.6$.

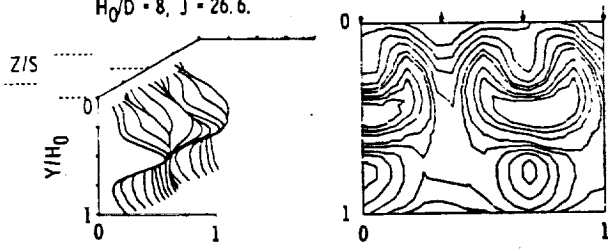

(d) Double row of staggered holes; $S_x/H_0 = 0.5$; Row 1: $S/H_0 = 1$, $H_0/D = 4$, $J = 26.8$. Row 2: $S/H_0 = 1$, $H_0/D = 4$, $J = 26.7$.

Figure 21. - Comparison of temperature distributions for double and single rows of jets at $X/H_0 = 0.5$ and intermediate momentum flux ratios; $A_j/A_m = 0.1$.

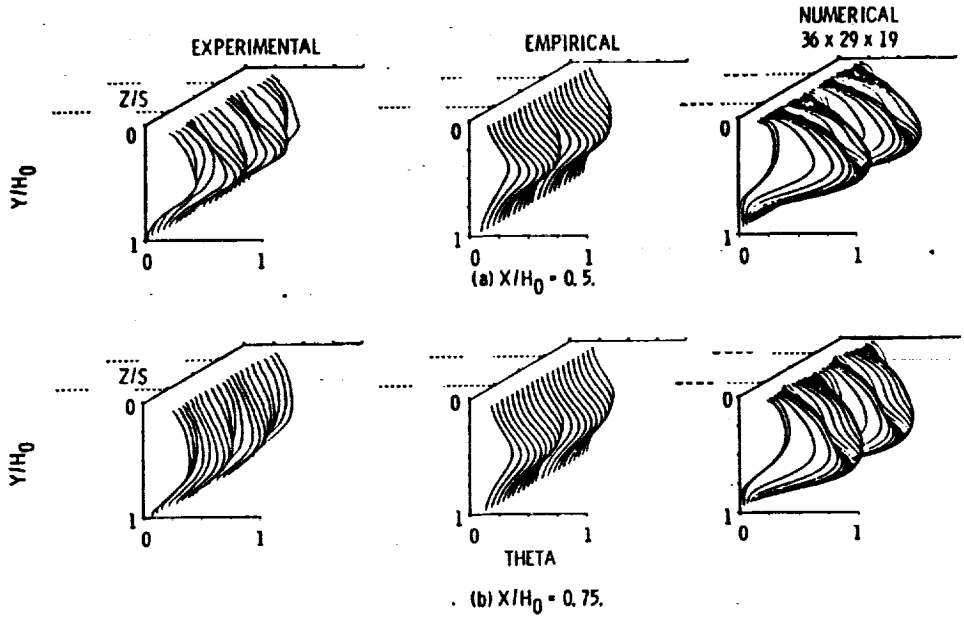

Figure 22. - Temperature distributions for a double row of in-line jets (A_j/A_m = 0.10, S_x/H_0 = 0.5; Row 1: S/H_0 = 0.5, H_0/D = 5.7, J = 26.3; Row 2: S/H_0 = 0.5, H_0/D = 5.7, J = 26.9).

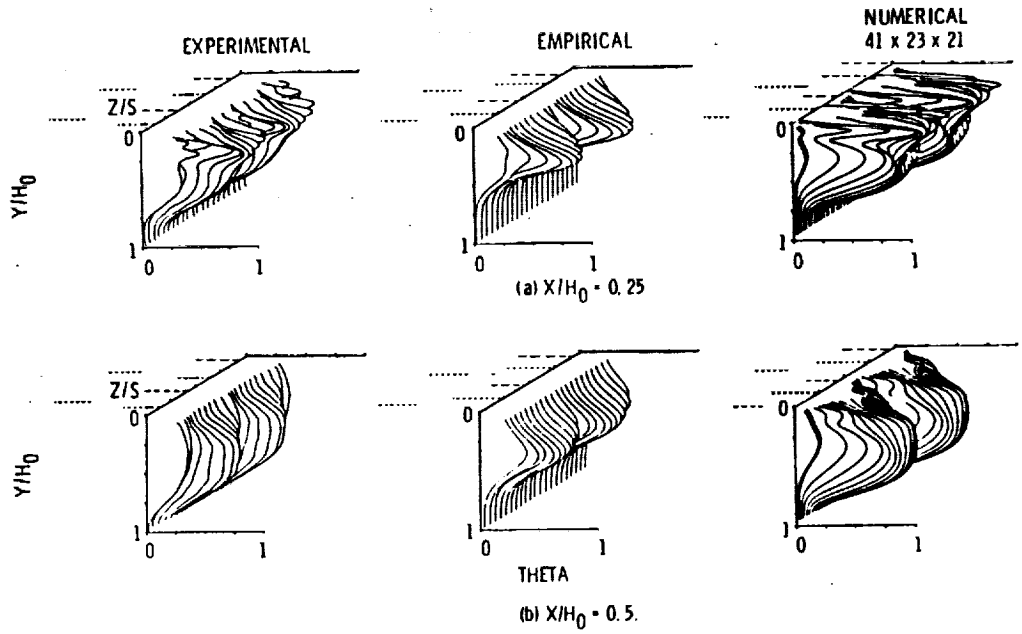

Figure 23. - Temperature distribution for a double row of disimilar jets (A_j/A_m = 0.10, S_x/H_0 = 0.25; Row 1: S/H_0 = 0.5, H_0/D = 5.7, J = 26.8; Row 2: S/H_0 = 0.25, H_0/D = 8, J = 26.6).

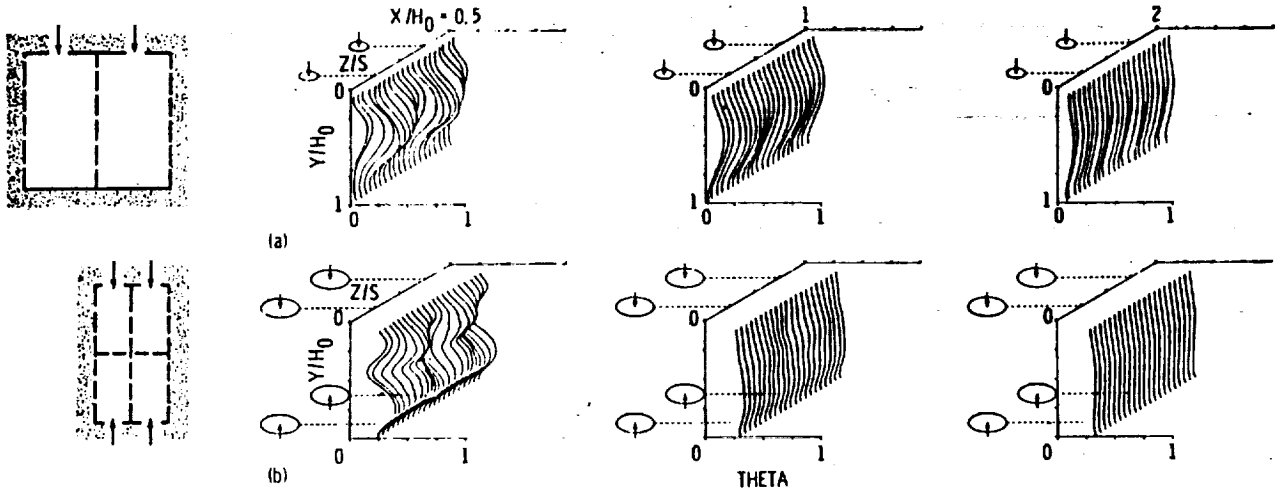

(a) Single-side (top) injection: $S/H_o = 0.5$, $A_j/A_m = .025$, $J = 28.4$.

(b) Opposed row (in-line) injection: $S/H_o = 0.25$, $A_j/A_m = 0.10$, $J = 25.0$.

Figure 24.—Comparison between single-side and opposed jet injection ($H_o/D = 8$).

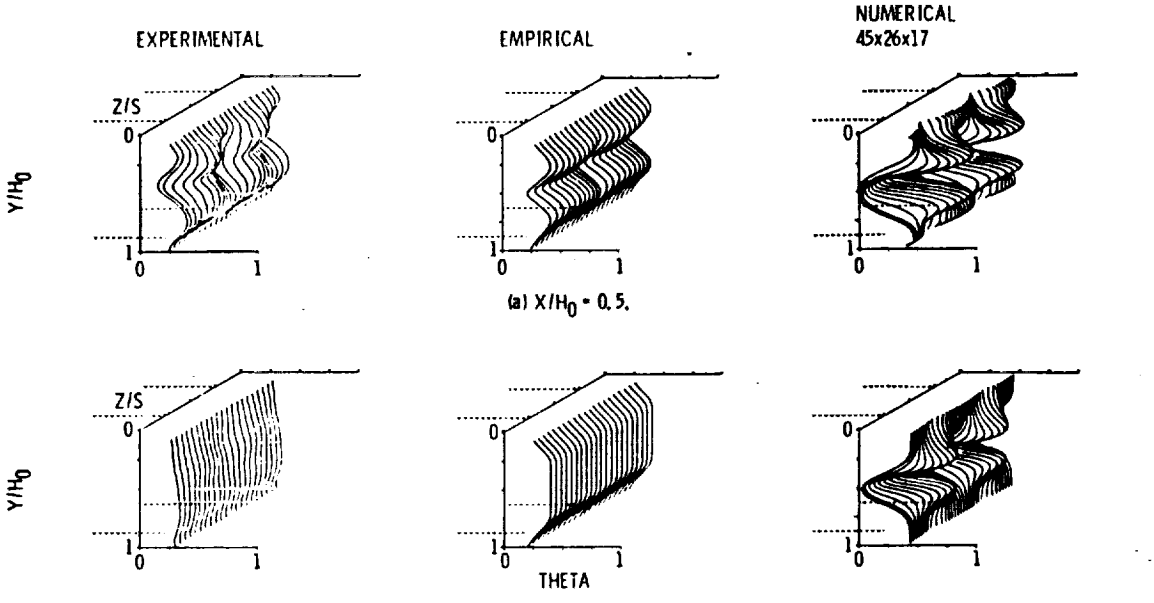

Figure 25 - Temperature distributions for opposed rows of in-line jets ($S/H_0 = 0.25$, $H_0/D = 8$, $A_j/A_m = 0.10$, $J = 25$).

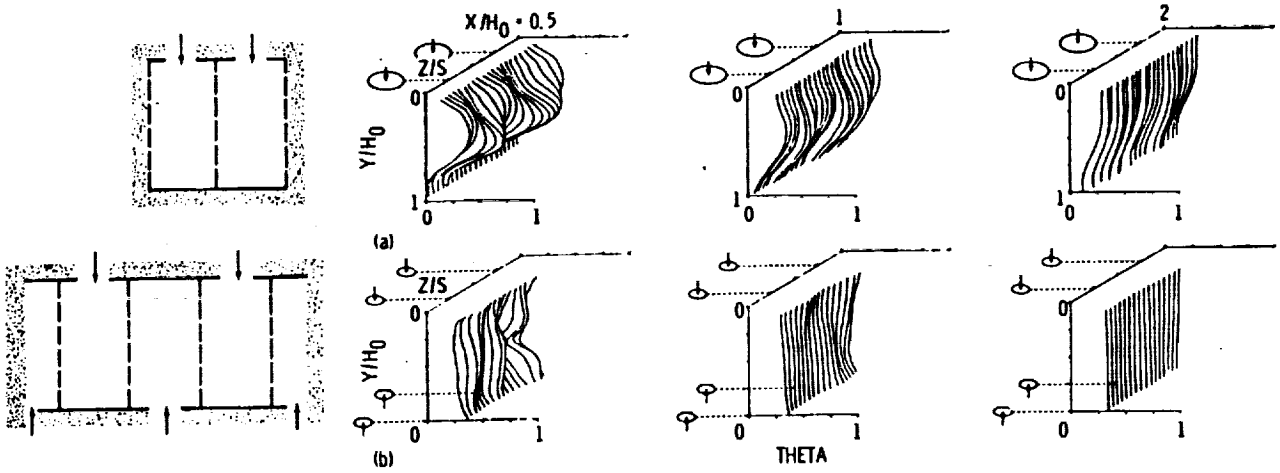

(a) Single-side (top) injection: S/H_o = 0.5, J = 18.6.

(b) Opposed row (staggered) injection: S/H_o = 1, J = 27.6.

Figure 26.—Comparison between single-side and staggered jet injection (H_o/D = 4; A_j/A_m = 0.10).

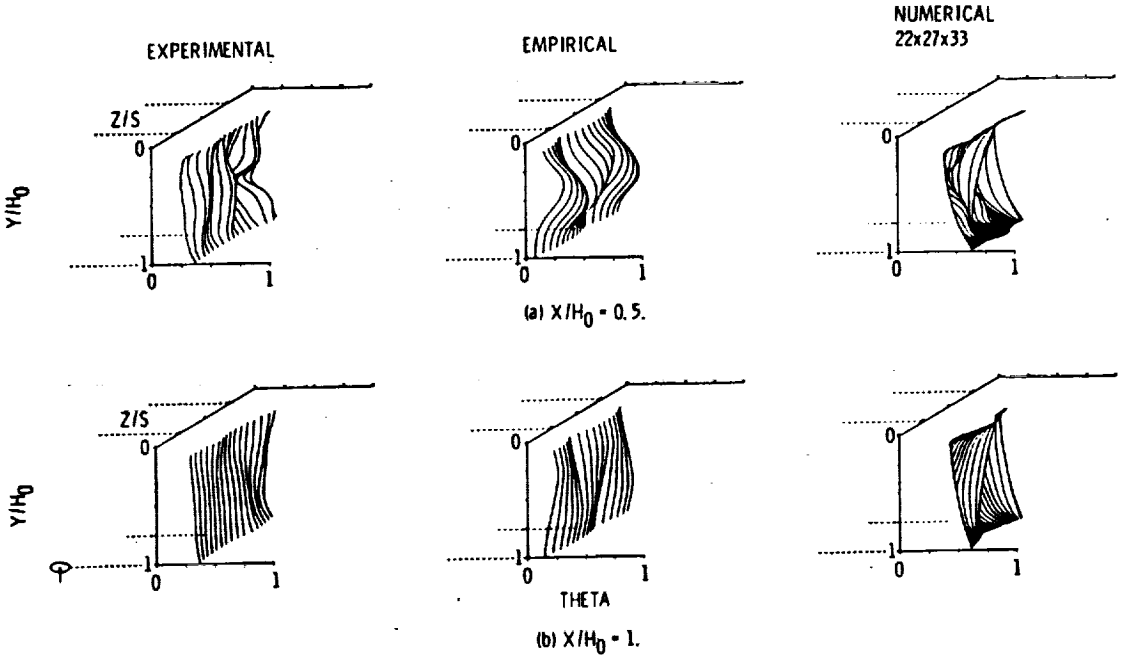

(a) X/H_0 = 0.5.

(b) X/H_0 = 1.

Figure 27. - Temperature distributions for opposed rows of staggered jets (S/H_0 = 1, H_0/D = 4, A_j/A_m = 0.10, J = 27.6).

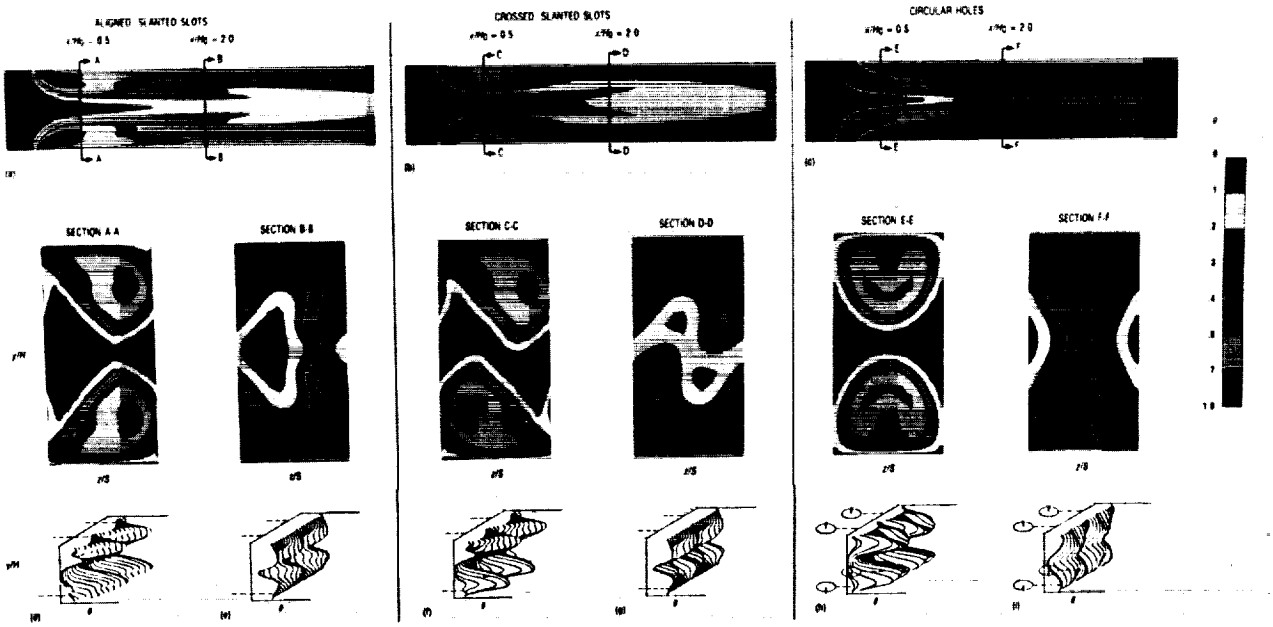

Figure 28.—Numerical model calculations of temperature distributions for opposed rows of staggered jets ($S/H_o = 0.5$, $H_o/D = 4$, $A_j/A_m = 0.10$, $J = 6.6$).

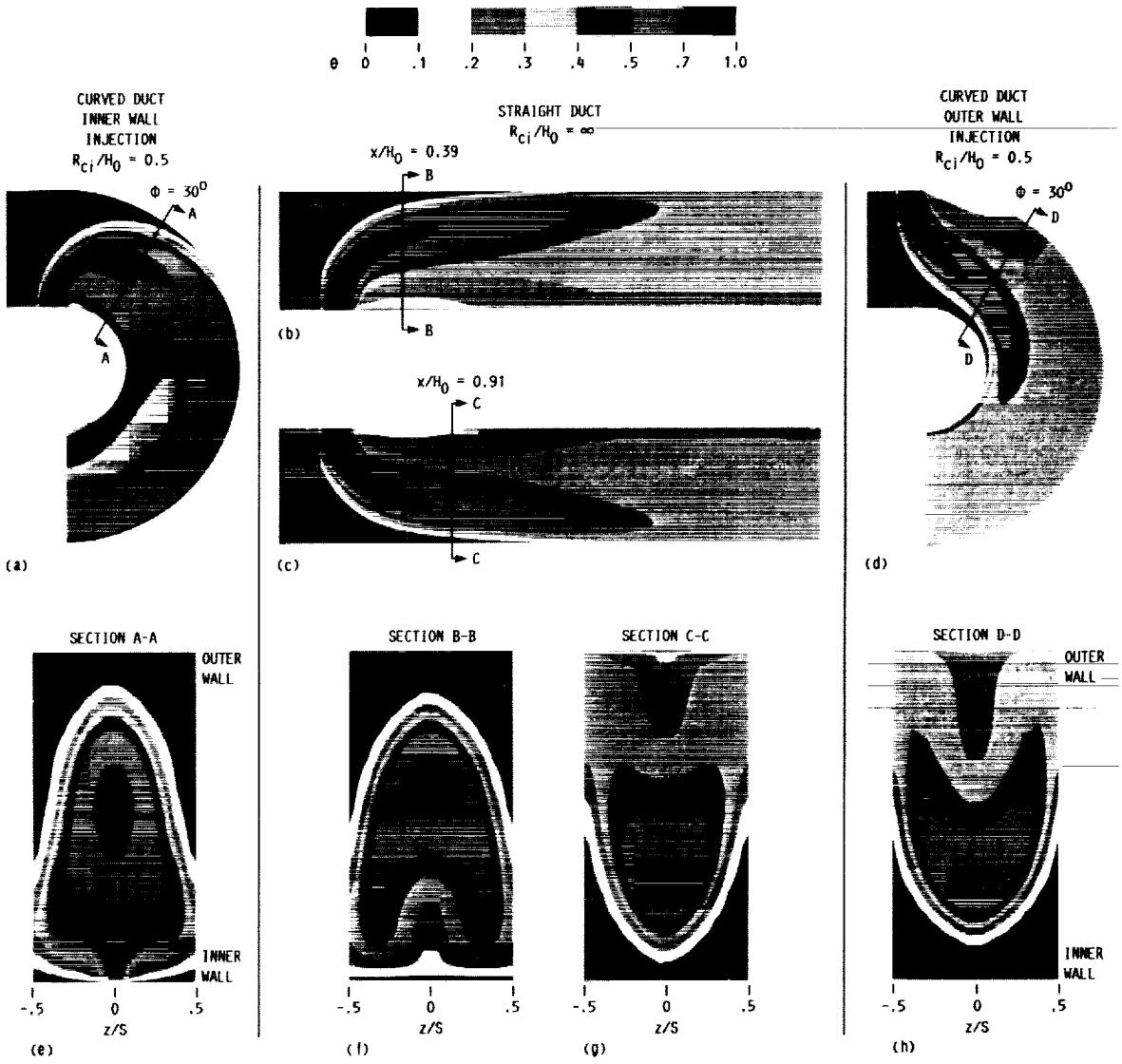

Figure 29.—Numerical calculations of temperature field downstream of jets injected from inner and outer walls in straight and curved ducts (J = 26.4, S/H_0 = 0.5, H_0/D = 4, R_1/H_0 = infinity).

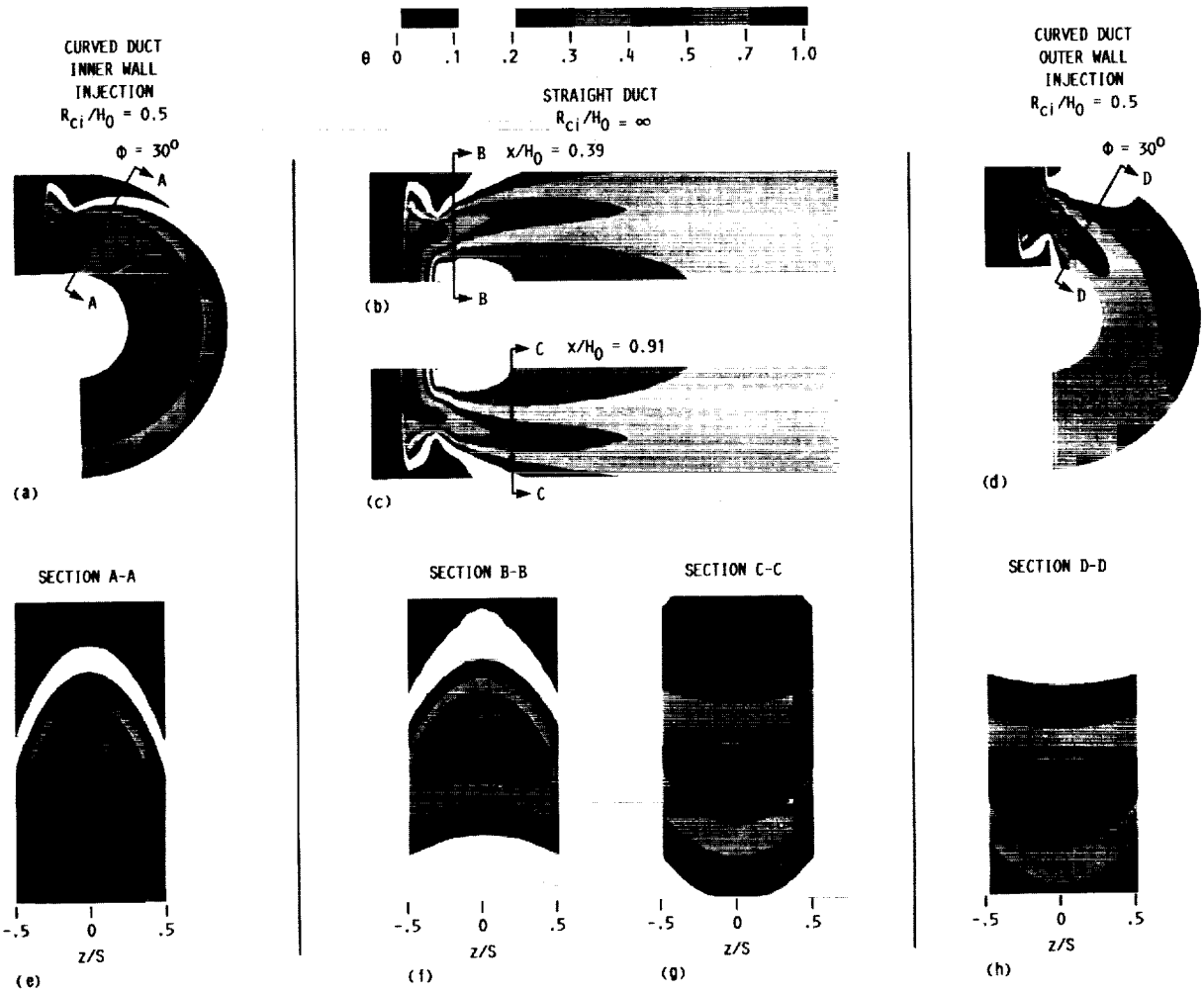

Figure 30.—Empirical model calculations of temperature field downstream of jets injected from inner and outer walls in straight and curved ducts (J = 26.4, S/H_0 = 0.5, H_0/D = 4, R_t/H_0 = infinity).

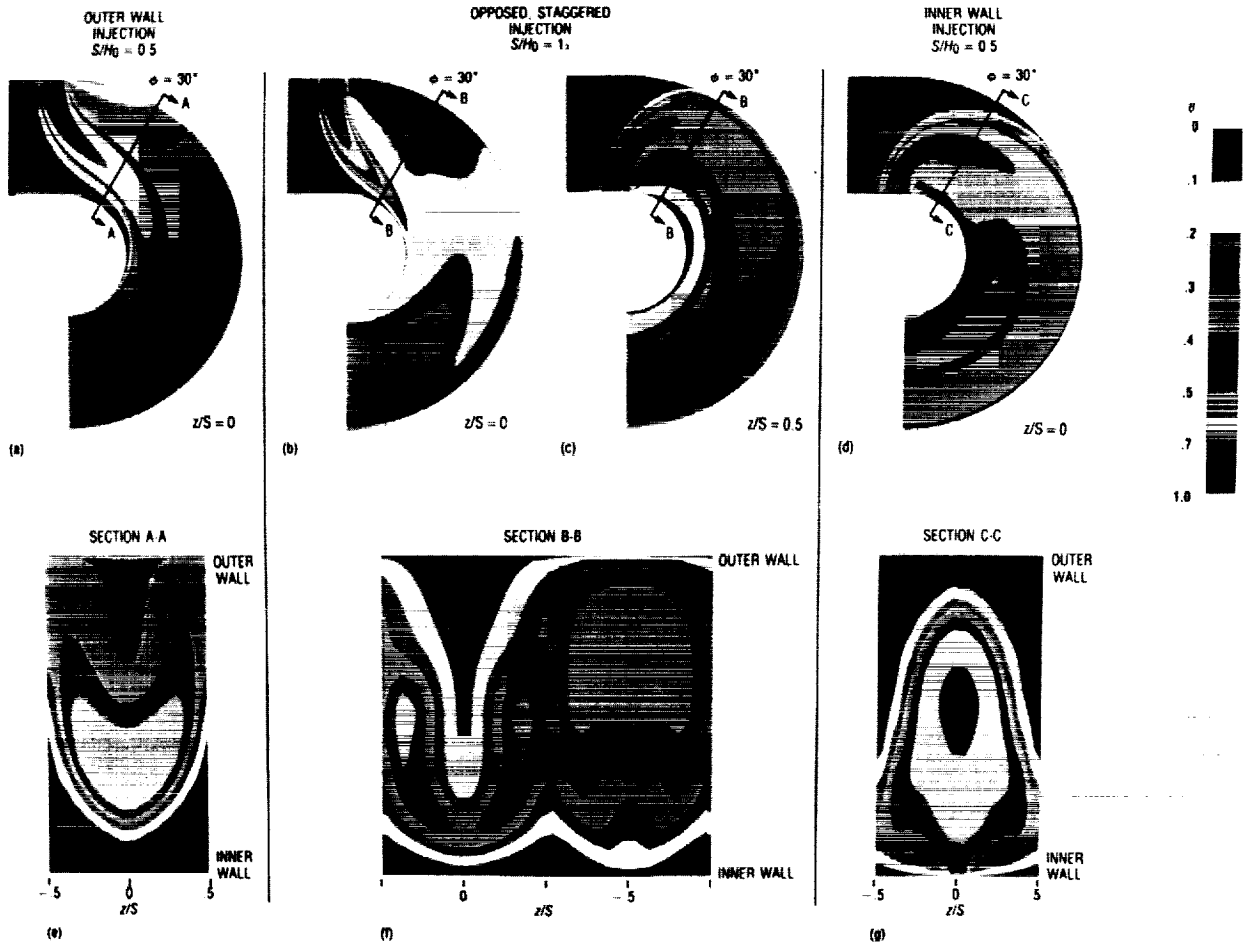

Figure 31.—Numerical model calculations for opposed rows with jet centerlines staggered (J = 26.4, H_o /D = 4, R_{ci} /H_o = 0.5, R_t /H_o = infinity).

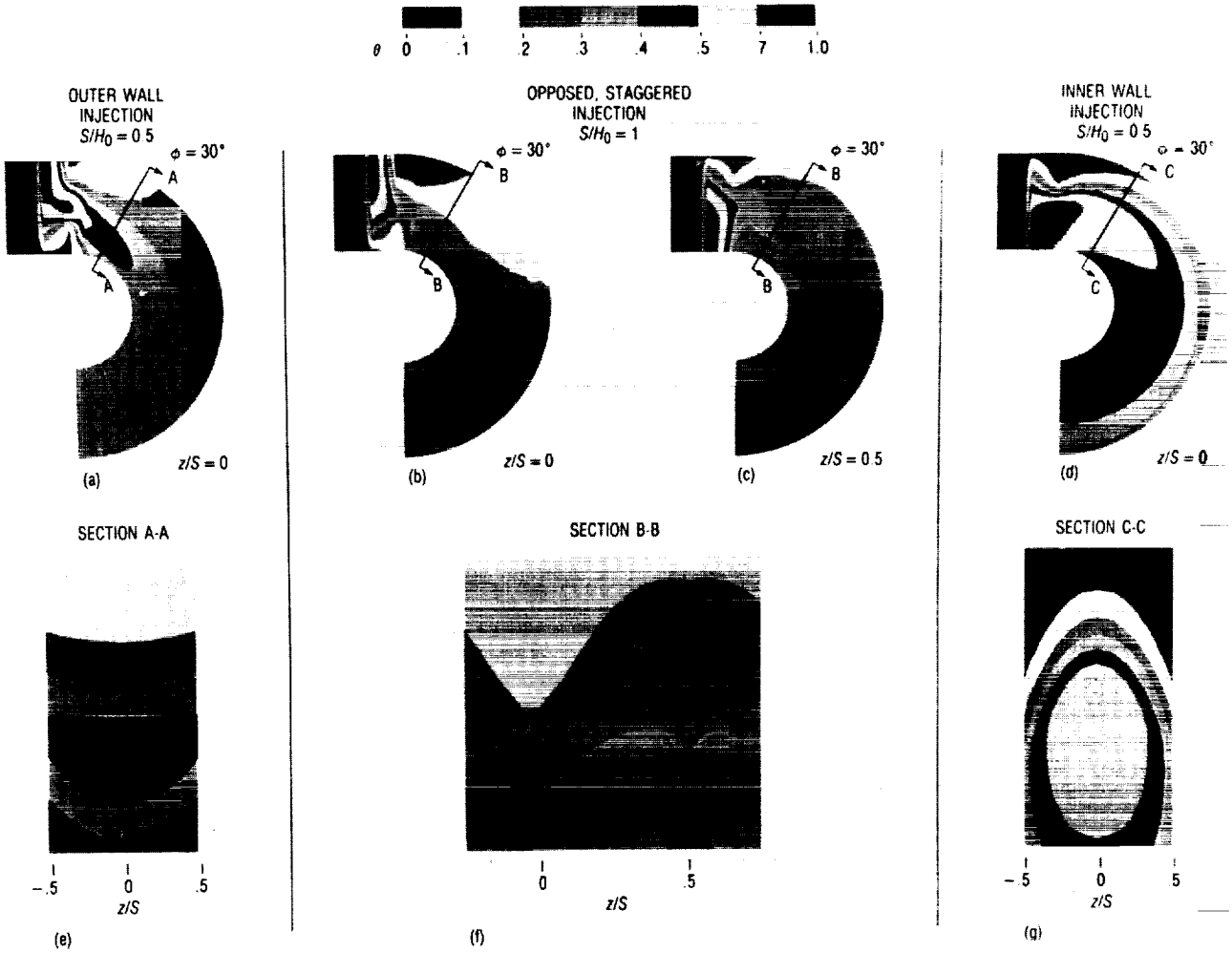

Figure 32.—Empirical model calculations for opposed rows with jet centerlines staggered ($J = 26.4$, $H_o/D = 4$, $R_{ci}/H_o = 0.5$, R_t/H_o = infinity).

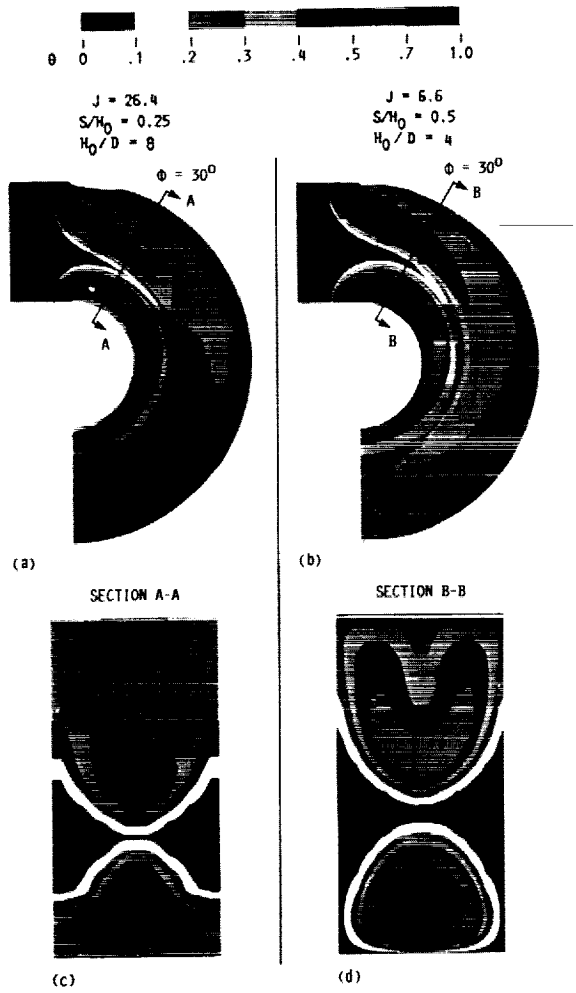

Figure 33.—Numerical model calculations for opposed rows with jet centerlines in-line (R_{ci}/H_o = 0.5, R_t/H_o = infinity).

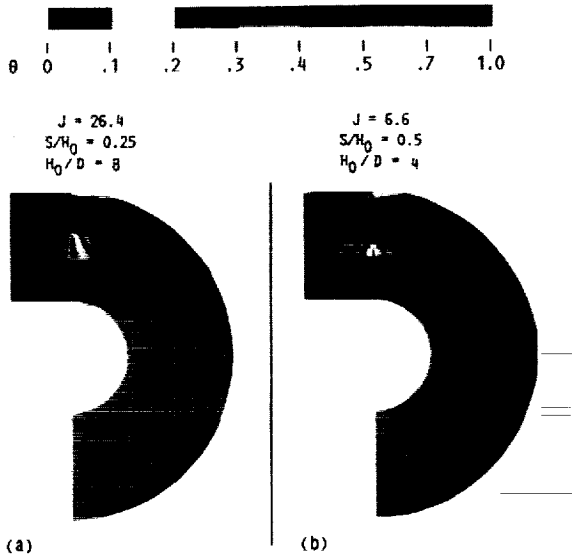

Figure 34.—Empirical model calculations for opposed rows with jet centerlines in-line (R_{ci}/H_o = 0.5, R_t/H_o = infinity).

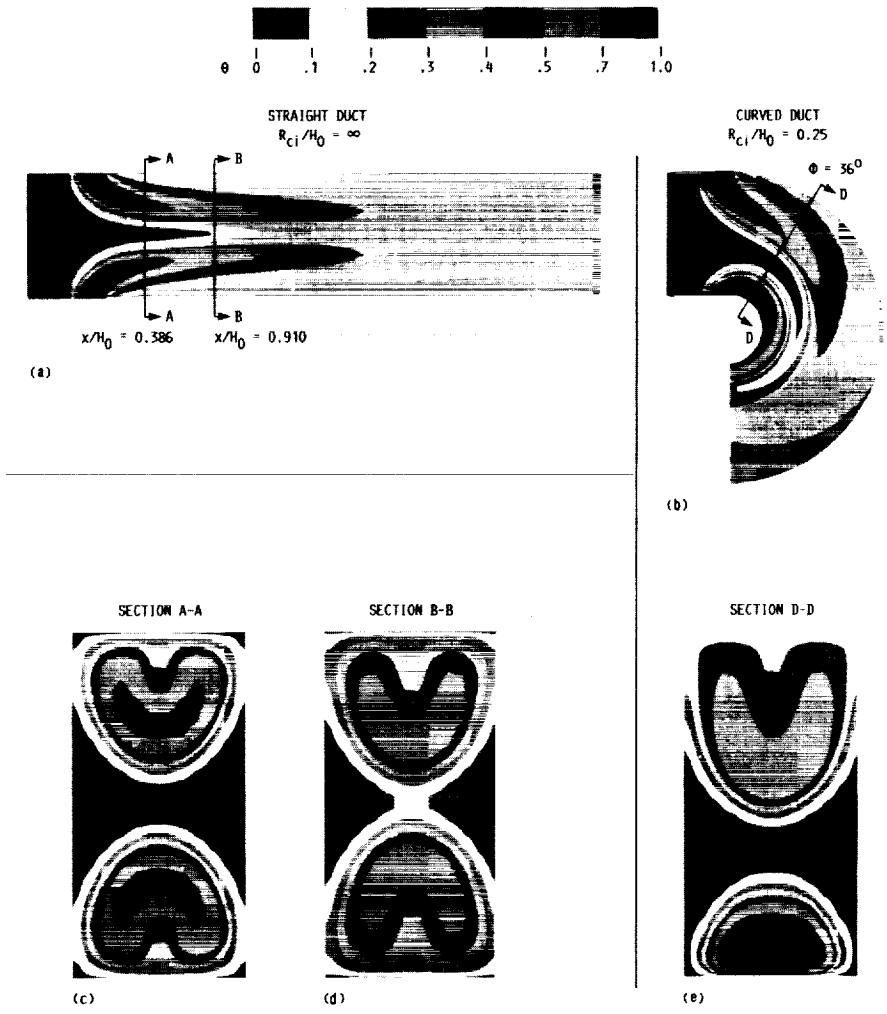

Figure 35.—Numerical model calculations showing effect of radius of curvature in x-r plane (J = 6.6, S/H_0 = 0.5, H_0/D = 4, R_t/H_0 = infinity).

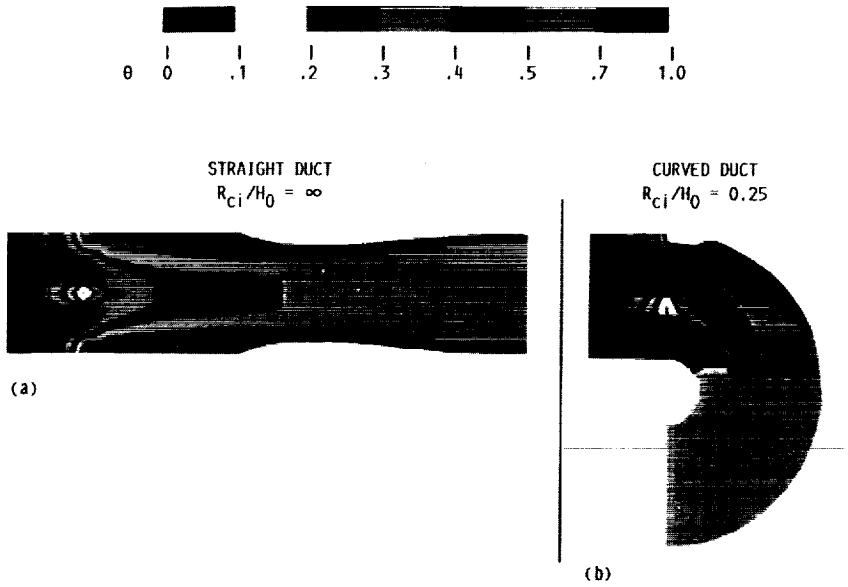

Figure 36.—Empirical model calculations showing effect of radius of curvature in x-r plane (J = 6.6, $S/H_0 = 0.5$, $H_0/D = 4$, R_t/H_0 = infinity).

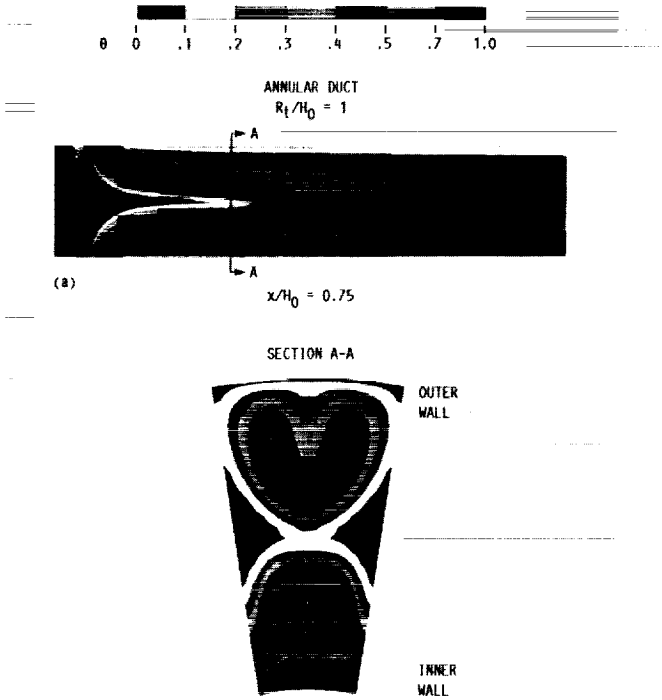

Figure 37.—Numerical model calculations for the mixing of jets in an annular duct (J = 6.6, $S/H_0 = 0.5$, $H_0/D = 4$, R_{Ci}/H_0 = infinity).

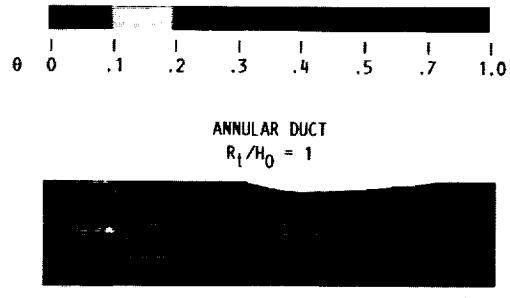

Figure 38.—Empirical model calculations for the mixing of jets in an annular duct (J = 6.6, $S/H_0 = 0.5$, $H_0/D = 4$, R_{Ci}/H_0 = infinity).

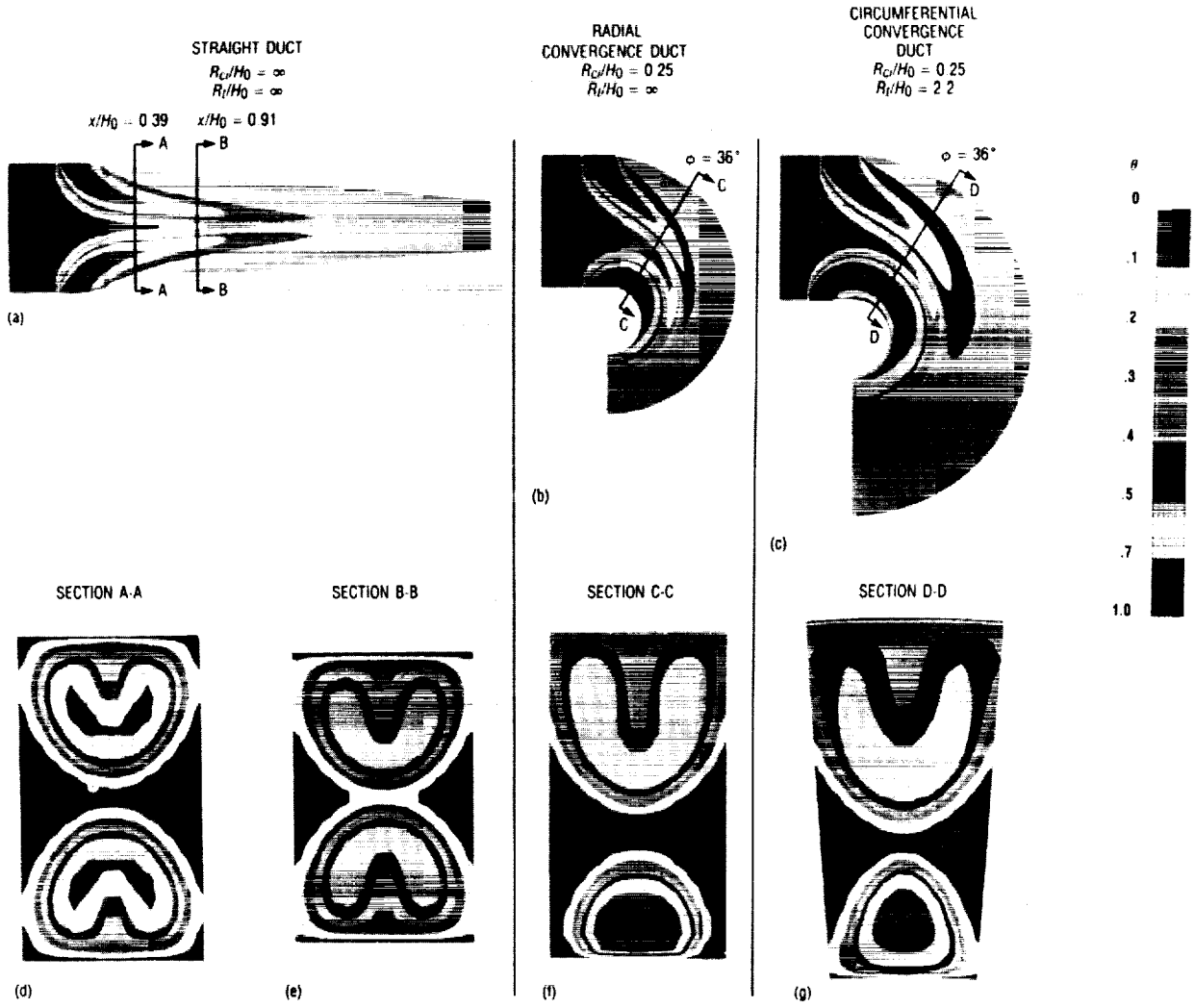

Figure 39.—Numerical model calculations showing the effect of convergence; exit: inlet area ratio = 1.3.

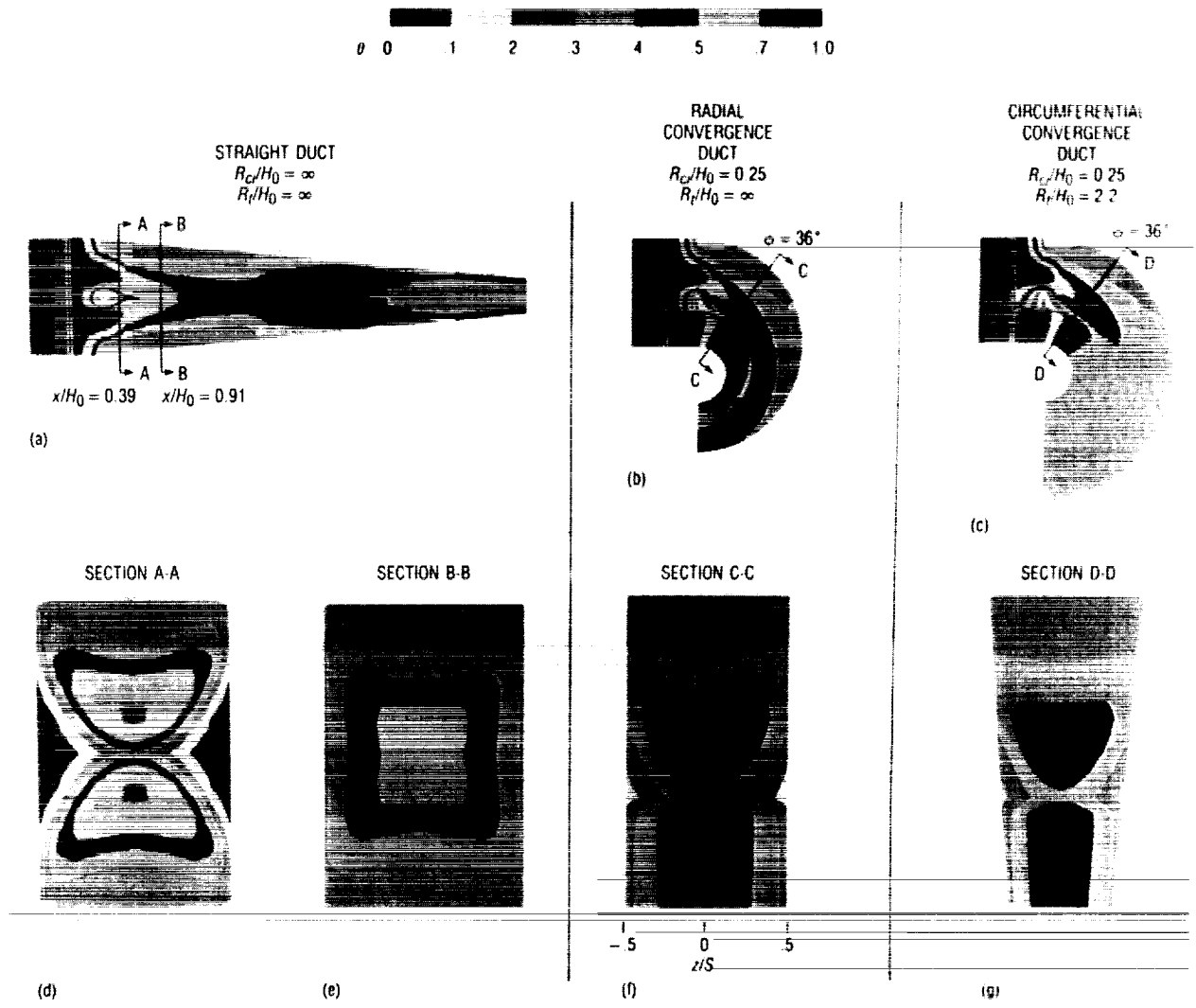

Figure 40.—Empirical model calculations showing the effect of convergence; exit: inlet area ratio = 1.3.

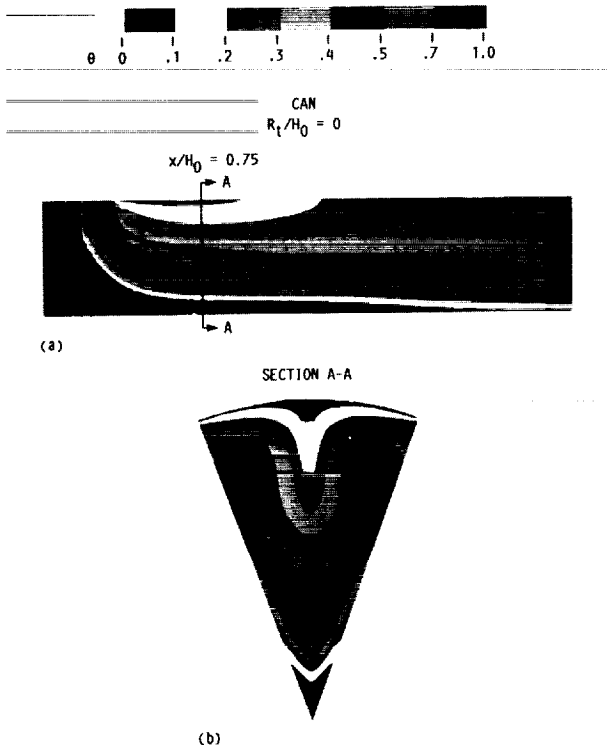

Figure 41.—Numerical model calculations for the mixing of jets injected into a can (J = 26.4, S/H_0 = 0.5, H_0/D = 4, R_{ci}/H_0 = infinity, R_1/H_0 = infinity).

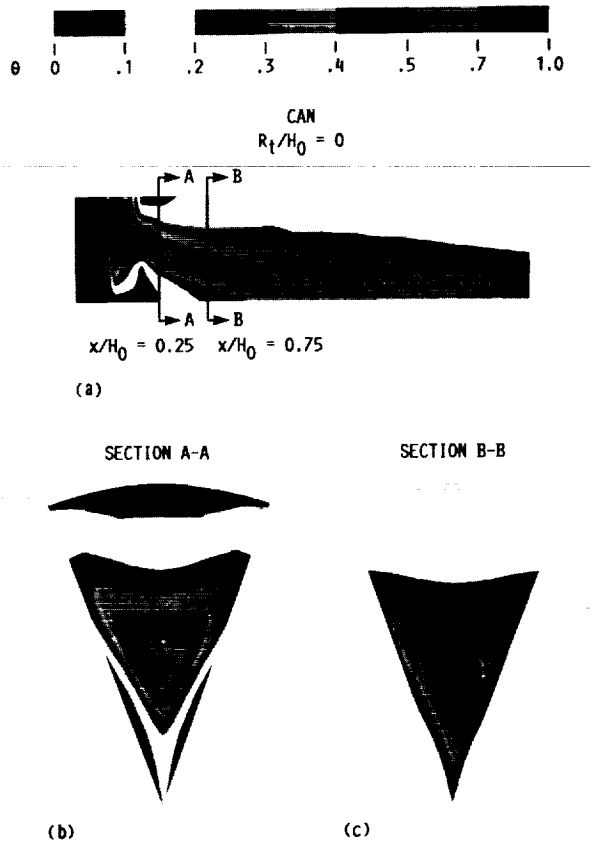

Figure 42.—Empirical model calculations for the mixing of jets injected into a can (J = 26.4, S/H_0 = 0.5, H_0/D = 4, R_{ci}/H_0 = infinity, R_t/H_0 = infinity).

NASA
National Aeronautics and Space Administration

Report Documentation Page

1. Report No.	2. Government Accession No.	3. Recipient's Catalog No.
NASA TM - 104412 AIAA - 91-2458		

4. Title and Subtitle
Mixing of Multiple Jets With a Confined Subsonic Crossflow
Summary of NASA-Supported Experiments and Modeling

5. Report Date

6. Performing Organization Code

7. Author(s)
James D. Holdeman

8. Performing Organization Report No.
E -6239

10. Work Unit No.
537 -02-21

9. Performing Organization Name and Address
National Aeronautics and Space Administration
Lewis Research Center
Cleveland, Ohio 44135 - 3191

11. Contract or Grant No.

13. Type of Report and Period Covered

12. Sponsoring Agency Name and Address
National Aeronautics and Space Administration
Washington, D.C. 20546 - 0001

14. Sponsoring Agency Code

15. Supplementary Notes
Prepared for the 27th Joint Propulsion Conference cosponsored by AIAA, SAE, ASME, and ASEE, Sacramento, California, June 24-27, 1991. Responsible person, James D. Holdeman, (216) 433-5846.

16. Abstract

This paper summarizes experimental and computational results on the mixing of single, double, and opposed rows of jets with an isothermal or variable temperature mainstream in a confined subsonic crossflow. The studies from which these results came were performed to investigate flow and geometric variations typical of the complex 3-D flowfield in the dilution zone of combustion chambers in gas turbine engines. The principal observations from the experiments were that the momentum-flux ratio was the most significant flow variable, and that temperature distributions were similar, independent of orifice diameter, when the orifice spacing and the square-root of the momentum-flux ratio were inversely proportional. The experiments and empirical model for the mixing of a single row of jets from round holes were extended to include several variations typical of gas turbine combustors, namely variable temperature mainstream, flow area convergence, non-circular orifices, and double and opposed rows of jets, both in-line and staggered. All except the last of these were appropriately modelled with superposition or patches to the basic empirical model. Combinations of flow and geometry that gave optimum mixing were identified from the experimental results. Based on the results of calculations made with a three-dimensional numerical model, the empirical model was further extended to model the effects of curvature and convergence. The principal conclusions from this study were that the orifice spacing and momentum-flux relationships were the same as observed previously in a straight duct, but the jet structure was significantly different for jets injected from the inner wall of a turn than for those injected from the outer wall. Also, curvature in the axial direction caused a drift of the jet trajectories toward he inner wall, but the mixing in a turning and converging channel did not seem to be inhibited by the convergence, independent of whether the convergence was radial or circumferential. The calculated jet penetration and mixing in an annulus were similar to those in a rectangular duct when the orifice spacing was specified at the radius dividing the annulus into equal areas.

17. Key Words (Suggested by Author(s))	18. Distribution Statement
Dilution; Crossflow; Gas turbines; Jet mixing flow; Combustion Chambers	Unclassified - Unlimited Subject Category 07

19. Security Classif. (of the report)	20. Security Classif. (of this page)	21. No. of pages	22. Price*
Unclassified	Unclassified		

NASA FORM 1626 OCT 86

*For sale by the National Technical Information Service, Springfield, Virginia 22161